

Diffusion Domain Teacher: Diffusion Guided Domain Adaptive Object Detector

Boyong He*
Xiamen University
Institute of Artificial
Intelligence
Xiamen, China
boyonghe@stu.xmu.edu.cn

Yuxiang Ji*
Xiamen University
Institute of Artificial
Intelligence
Xiamen, China
yuxiangji@stu.xmu.edu.cn

Zhuoyue Tan
Xiamen University
Institute of Artificial
Intelligence
Xiamen, China
tanzhuoyue@stu.xmu.edu.cn

Liaoni Wu†
Xiamen University
Institute of Artificial
Intelligence
School of Aerospace
Engineering
Xiamen, China
wuliaoni@xmu.edu.cn

Abstract

Object detectors often suffer a decrease in performance due to the large domain gap between the training data (source domain) and real-world data (target domain). Diffusion-based generative models have shown remarkable abilities in generating high-quality and diverse images, suggesting their potential for extracting valuable feature from various domains. To effectively leverage the cross-domain feature representation of diffusion models, in this paper, we train a detector with frozen-weight diffusion model on the source domain, then employ it as a teacher model to generate pseudo labels on the unlabeled target domain, which are used to guide the supervised learning of the student model on the target domain. We refer to this approach as *Diffusion Domain Teacher (DDT)*. By employing this straightforward yet potent framework, we significantly improve cross-domain object detection performance without compromising the inference speed. Our method achieves an average mAP improvement of 21.2% compared to the baseline on 6 datasets from three common cross-domain detection benchmarks (*Cross-Camera*, *Syn2Real*, *Real2Artistic*), surpassing the current state-of-the-art (SOTA) methods by an average of 5.7% mAP. Furthermore, extensive experiments demonstrate that our method consistently brings improvements even in more powerful and complex models, highlighting broadly applicable and effective domain adaptation capability of our DDT. The code is available at <https://github.com/heboyong/Diffusion-Domain-Teacher>.

Keywords

Unsupervised domain adaptation; Object detection; Diffusion model

* Contribute equally to the work.

† Corresponding author.

Permission to make digital or hard copies of all or part of this work for personal or classroom use is granted without fee provided that copies are not made or distributed for profit or commercial advantage and that copies bear this notice and the full citation on the first page. Copyrights for components of this work owned by others than the author(s) must be honored. Abstracting with credit is permitted. To copy otherwise, or republish, to post on servers or to redistribute to lists, requires prior specific permission and/or a fee. Request permissions from permissions@acm.org.
MM '24, October 28-November 1, 2024, Melbourne, VIC, Australia

© 2024 Copyright held by the owner/author(s). Publication rights licensed to ACM.
ACM ISBN 979-8-4007-0686-8/24/10
<https://doi.org/10.1145/3664647.3680962>

ACM Reference Format:

Boyong He, Yuxiang Ji, Zhuoyue Tan, and Liaoni Wu. 2024. Diffusion Domain Teacher: Diffusion Guided Domain Adaptive Object Detector. In *Proceedings of the 32nd ACM International Conference on Multimedia (MM '24)*, October 28-November 1, 2024, Melbourne, VIC, Australia. ACM, New York, NY, USA, 22 pages. <https://doi.org/10.1145/3664647.3680962>

1 Introduction

Object detection is a fundamental task in computer vision, with its applications permeating an array of real-world scenarios. There have been impressive strides and significant achievements in object detection, leveraging both Convolutional Neural Networks (CNNs) [45, 57, 58, 72] and transformer-based models [4, 92]. Nonetheless, these data-driven detection algorithms wrestle with the challenging issue of domain shift: the large gap between the training data (source domain) and the testing environments (target domain) frequently results in a substantial decline in detection accuracy. This obstacle is ubiquitous across various sectors, including robotics, autonomous driving, and healthcare, and it poses a formidable barrier to the widespread applications of object detection in practice. Consequently, the deployment of domain adaptation techniques, aimed at minimizing domain disparities, has become essential to boost the robustness and generalizability of models across diverse environments.

Unsupervised Domain Adaptation (UDA) methodologies have surged to the forefront of research, taking advantage of the sparse labeled data from the source domain in conjunction with copious unlabeled data from the target domain to significantly enhance cross-domain detection performance. Current UDA tactics have explored a variety of strategies including domain classifiers [11, 27, 64, 88, 91], graph matching [39, 41, 42], domain randomization [34], image-to-image translation [28], and self-training frameworks [6, 15, 44, 61]. These techniques have been crucial in achieving notable advancements in cross-domain object detection.

Moreover, diffusion-based generative models [25, 59, 67] have showcased remarkable capabilities in generating high-quality and diverse images, signaling their vast potential for a spectrum of downstream applications. Some works [1, 73, 78] have already harnessed diffusion models for a breadth of tasks. This evidence suggests a promising avenue for employing these models to bolster cross-domain detection efficacy. Nevertheless, the step-by-step inference process of these models is not fast enough to meet the immediate processing needs of object detection. Although there

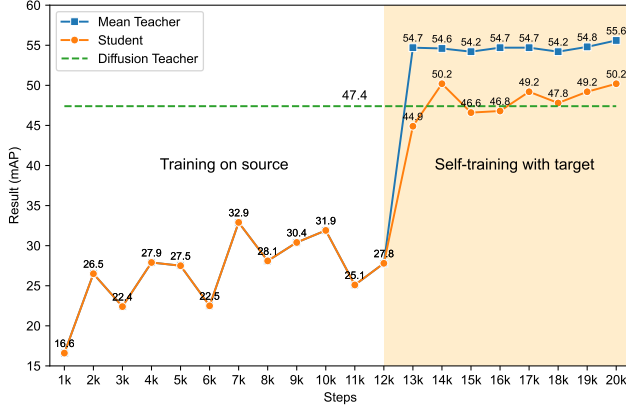


Figure 1: Evaluation results on Clipart [30] during training. It is evident that the performance of the **student** significantly improves after entering self-training, even surpassing the **diffusion teacher**, and the **mean teacher** exhibits better performance compared to the student.

has been some effort to adapt diffusion models for image generation and manipulation, as seen with tools like LoRA [29] and Control-Net [83], there is a lack of research on applying diffusion models to cross-domain detection.

Fortunately, current UDA methods provide us with valuable insights. Specifically, we draw inspiration from previous state-of-the-art (SOTA) approaches [3, 15, 44] and adopt the Mean Teacher [71] self-training framework, where the teacher model generates pseudo labels for the supervised learning of student model on the target domain. The weights of the teacher model are typically updated through Exponential Moving Average (EMA) by the student model. This consistency-based self-training approach allows the student model to progressively learn from the target domain, thereby improving the performance of the detector in cross-domain detection.

In our approach, we freeze all parameters of the diffusion model and extract intermediate feature from the upsampling structure of the U-Net [60] architecture during the inversion process. These features are then passed through a bottle-neck structure to generate hierarchical features similar to a general backbone for downstream detection tasks. This enables effective training and fine-tuning of the diffusion model with a small number of parameters, and yields discriminative feature for classification and regression tasks, leading to improved performance in cross-domain detection. The mean teacher, updated through EMA from the student model, further enhances stability and generalization.

Through the detector with the diffusion backbone for feature extraction struggles to match or surpass the performance of general backbones like ResNet [23] on intra-domain. However, in the target domain, the performance of the diffusion detector surpasses them greatly. This strongly confirms the diffusion model is an incredibly powerful and highly generalized feature extractor. Furthermore, it is even more remarkable that the diffusion teacher model continues to enhance the cross-domain performance of stronger backbones, all without any increase in additional inference speed.

The contributions of this paper can be summarized as follows:

- We introduce a frozen-weight diffusion model as backbone, which efficiently extracts highly generalized and discriminative feature for cross-domain object detection. Notably, the diffusion-based detector, trained exclusively on the source domain, demonstrates exceptional performance when applied to the target domain.
- We incorporate the diffusion detector as a teacher model within the self-training framework, providing valuable guidance supervised learning of the student model on the target domain. This integration effectively enhances cross-domain detection performance without any increasing of inference time.
- We achieve substantial improvements in cross-domain detection. Our method achieves an average mAP improvement of 21.2% compared with the baseline, and surpassing the current SOTA methods by 5.7% mAP. Further experiments demonstrate that the diffusion domain teacher consistently enhances cross-domain performance for detectors with stronger backbones, leading to superior results in the target domain.

2 Related Work

2.1 Object Detection

Object detection aims to locate and classify objects in given images. Deep convolutional neural networks [23, 66] have revolutionized this task and is widely applied in real-world applications. Faster R-CNN [58], a prominent two-stage detection method, employs a region proposal network (RPN) to generate candidate regions, followed by region of interest (ROI) refinement to determine the final bounding boxes and classes. Some research is focused on improving the precision and efficiency of two-stage methods [2, 55]. In addition, researchers are investigating single-stage detectors [45, 57, 74] aimed at simplifying the detection process by integrating box regression and classification. Moreover, anchor-free detectors [72, 84] that eliminate the reliance on predefined anchors have garnered significant attention. Recent research trends involve the adoption of transformer-based end-to-end detectors [4, 82, 92], which reconceptualize the detection task as a set prediction problem, thereby obviating the necessity for traditional handcrafted components such as anchor generation and non-maximum suppression (NMS).

2.2 Domain adaptation Detection

Although object detection has made significant advancements, performance can suffer greatly due to domain shifts between training and test data. To address this issue, UDA aims to mitigate the impact of domain shifts by leveraging labeled source data and unlabeled target data. Initially, studies inspired by GANs [20] introduced domain adversarial training [18], which minimized domain gaps by extracting invariant feature. This approach is later adapted to detection tasks [11, 27, 64, 88, 91], resulting in notable improvements in performance on the target domain. Some methods [28] focus on reducing inter-domain differences at image level, by applying image-to-image translate like CycleGAN [90].

Recently, self-training domain adaptation methods [3, 14, 15, 44] have achieved better results in cross-domain object detection by optimizing the learning of pseudo labels in the target domain. For

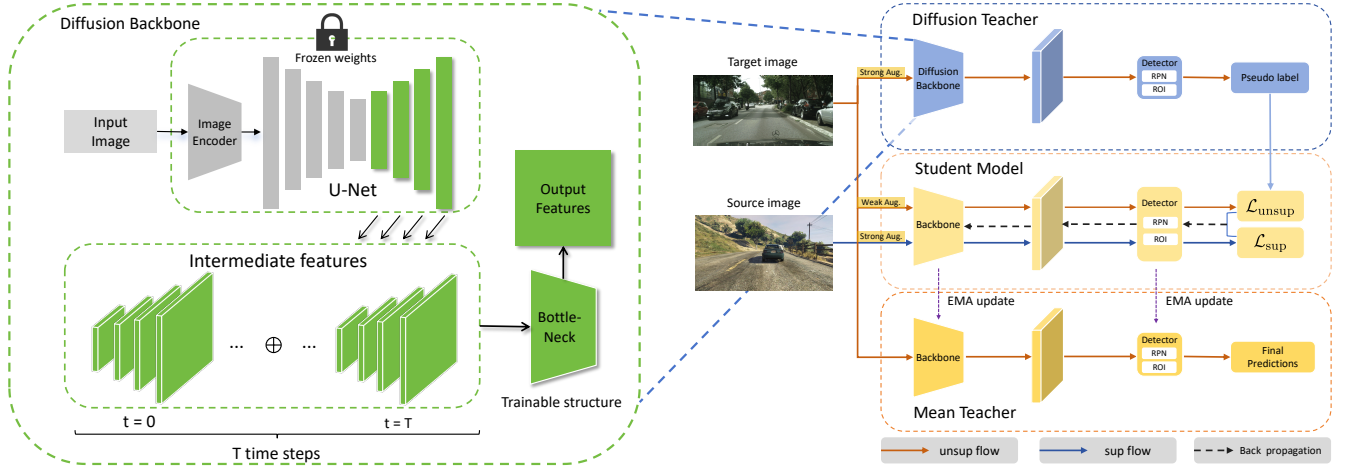


Figure 2: Overview of our proposed Diffusion Domain Teacher (DDT). Left: We employ a frozen-weight diffusion model with bottleneck as the **diffusion backbone**, which acquires and aggregates intermediate feature from the U-Net [60] during the inversion process at T time steps for detection. Right: We use the **diffusion teacher**, which is a detector with the diffusion backbone, and applied it in self-training to generate pseudo labels for unlabeled target, guiding the learning of the student. By EMA updated from the student model, **mean teacher** is refined and serves as the final model, resulting in improved cross-domain detection results.

example, AT [44] combines domain adversarial training and self-training to improve the quality of pseudo labels. UMT [14] utilizes consistency learning for a teacher model to generate high-quality pseudo labels to improve cross-domain detection. CMT [3] introduces contrastive learning to optimize the utilization and alignment of features from the source and target domain. HT [15] optimizes the generation of pseudo labels by applying consistency measures in regression and classification. Overall, self-training methods in cross-domain object detection enhance the detection performance in the target domain by improving the quality of pseudo labels, with the teacher model being updated from the student model.

2.3 Diffusion Models

Diffusion models [25, 56, 59, 63, 67] have achieved impressive results in image generation, surpassing previous models like GAN [20]. With their strong generative and generalization capabilities, some research has begun to explore the potential of diffusion models in feature representation and their application to downstream tasks. For instance, DDPMseg [1] and ODISE [78] utilize feature extracted from diffusion models for semantic and panoptic segmentation tasks, respectively. DIFT [69] and HyperFeature [53] use the diffusion model to discover correspondences in images. This inspires us to consider the application of diffusion models for improving cross-domain detection tasks.

3 Approach

In this section, we present our Diffusion Domain Teacher (DDT) framework in detail. First, in Sec. 3.1, we review the formulation of Unsupervised Domain Adaptation Detection (UDAD). Then, in Sec. 3.2, we provide a detailed description of how the frozen-weight diffusion model serves as a feature extractor, producing hierarchical features, to adapt to the detection task. Furthermore, in Sec. 3.3,

we explain the application of the diffusion teacher detector in the self-training framework, where pseudo labels generated on the unlabeled target domain guide the supervised learning of the student model. Finally, we summarize the total training objective.

3.1 Formulation of Unsupervised Domain adaptation Detection

To be specific, we denote a given set of N_s samples $\mathcal{S} = \{X_s^i, Y_s^i\}_{i=1}^{N_s}$ as source domain, where X_s^i represents an image and Y_s^i represents the bounding box with category labels in the respective image. Similarly, we denote the target domain data as $\mathcal{T} = \{X_t^i\}_{i=1}^{N_t}$, which consists of N_t unlabeled samples. Exactly, the distribution of \mathcal{S} and \mathcal{T} , including the distributions of images from $P(X_s)$ and $P(X_t)$ (e.g., style, scene, weather), labels $P(Y_s)$ and $P(Y_t)$ (e.g., the shapes, sizes, and density of instance), and even the scales of N_s and N_t are different, denoted as $P(\mathcal{S}) \neq P(\mathcal{T})$, is what we refer to as a cross-domain detection problem. Furthermore, relying solely on supervised learning from the labeled source domain results in an inherent bias towards source domain in cross-domain detection. Domain adaptation for detection aims to improving the performance on the target domain by reducing the dissimilarity between \mathcal{S} and \mathcal{T} , seeking to a domain-invariant detector.

3.2 Frozen-Diffusion Feature Extractor

Diffusion generative models [25, 59, 67] aim to minimize the discrepancy between the distribution of images generated by the model, denoted as $P_\theta(x)$, and the distribution of the training data, denoted as $P_{\text{data}}(x)$. During training, gaussian noise of varying magnitudes is added to the clean training data, commonly referred to as *diffusion* process. The diffusion process starts with a clean image x_0 from the training data and generates a noisy image x_t by mixing

x_0 with noise of different magnitudes:

$$x_t = \sqrt{\bar{\alpha}_t}x_0 + \sqrt{1 - \bar{\alpha}_t}\epsilon \quad (1)$$

where $\epsilon \sim \mathcal{N}(0, I)$ represents randomly sampled noise, and $t \in [0, T]$ denotes the time step, where larger values correspond to adding more noise. The amount of noise added is determined by α_t , which is a predefined noise schedule, and $\bar{\alpha}_t = \alpha_1 \alpha_2 \dots \alpha_t$. The model f_θ is trained to predict the input noise ϵ , given x_t and t , typically using structures like U-Net [60].

The iterative process of the diffusion model poses challenges when directly applied to downstream supervised tasks. We extract intermediate feature at a specific time step t during the inversion process, and apply these features for regression and classification tasks in the detection task. Specifically, we append a input noise corresponding the time step t to the input image, shift it to x_t and then input it along with t into f_θ to extract activation layers as intermediate feature. More specifically, we apply the intermediate feature from the four stages of the upsampling process in the de-noise network U-Net [60]. For each input image, we concatenate multiple time step feature together and employ a bottle-neck structure to project the feature into hierarchical layers with a channel size of [256, 512, 1024, 2048], similar to the output of ResNet [23], which is directly applied to the object detection task, as shown in the left side of Fig. 2.

3.3 Diffusion Teacher Guided Self-training Framework

We employ a detector that extracts feature using the diffusion model and trained on the source domain as the teacher model, denoted as $\mathcal{F}_{\text{diff}}$. It is used to generate pseudo labels \tilde{Y}_t on the target domain \mathcal{T} , where $\tilde{Y}_t = \mathcal{F}_{\text{diff}}(X_t)$. These pseudo labels are constructed to form a new dataset $\tilde{\mathcal{T}} = \{X_t^i, \tilde{Y}_t^i\}_{i=1}^{N_t}$. Subsequently, we optimize the student model using the pseudo labels. We introduce a hyper-parameter σ as a threshold for the confidence scores of the output for the teacher model, enabling us to select more reliable pseudo labels.

We define the supervised learning of the student model \mathcal{F}_{stu} on the source domain as follows:

$$\mathcal{L}_{\text{sup}}(X_s, Y_s) = \mathcal{L}_{\text{cls}}^{\text{RPN}}(X_s, Y_s) + \mathcal{L}_{\text{reg}}^{\text{RPN}}(X_s, Y_s) + \mathcal{L}_{\text{cls}}^{\text{ROI}}(X_s, Y_s) + \mathcal{L}_{\text{reg}}^{\text{ROI}}(X_s, Y_s) \quad (2)$$

where RPN is used to generate potential candidate regions, and ROI performs classification and bounding box regression on these candidate regions to obtain more accurate class and bounding box predictions, denoted as cls and reg, respectively. Similarly, we define the learning of the student model in the target domain as follows:

$$\mathcal{L}_{\text{unsup}}(X_t, \tilde{Y}_t) = \mathcal{L}_{\text{cls}}^{\text{RPN}}(X_t, \tilde{Y}_t) + \mathcal{L}_{\text{reg}}^{\text{RPN}}(X_t, \tilde{Y}_t) + \mathcal{L}_{\text{cls}}^{\text{ROI}}(X_t, \tilde{Y}_t) + \mathcal{L}_{\text{reg}}^{\text{ROI}}(X_t, \tilde{Y}_t) \quad (3)$$

Then, we employ EMA to update a mean teacher model $\mathcal{F}_{\text{mean}}$ by copying the weights from the student model. We define this process as follows:

$$\theta_t \leftarrow \alpha \theta_t + (1 - \alpha) \theta_s \quad (4)$$

where t and s represent the parameters of $\mathcal{F}_{\text{mean}}$ and \mathcal{F}_{stu} , respectively. By employing EMA to update the mean teacher model,

we aim to create a more stable and robust model by gradually incorporating the knowledge learned by the student model over time. We select the output of $\mathcal{F}_{\text{mean}}$ as result for predicting.

We apply a hyper parameter λ to adjust the weights between $\mathcal{L}_{\text{unsup}}$ and \mathcal{L}_{sup} . The final formulation of our comprehensive loss function is summarized as follows:

$$\mathcal{L} = \mathcal{L}_{\text{sup}} + \lambda \cdot \mathcal{L}_{\text{unsup}} \quad (5)$$

In our DDT framework, following [44], we employ *Weak Augmentation* to provide target domain images to the diffusion teacher model for generating reliable and accurate pseudo labels. Simultaneously, we apply *Strong Augmentation* to the images as inputs to the student model, as illustrated in Fig. 2. Specifically, *Weak Augmentation* includes random crop and random horizontal flip, while *Strong Augmentation* involves color transformations such as color space conversion, contrast adjustment, equalization, sharpness enhancement, and posterization, as well as spatial transformations such as rotation, shear, and translation of the position.

4 Experiments

4.1 Datasets

Cityscapes. Cityscapes [13] dataset provides a diverse of urban scenes from 50 cities. It includes 2,975 training images and 500 validation images with detailed annotations. The dataset covers 8 detection categories, using bounding boxes sourced from instance segmentation.

BDD100K. BDD100K [80] dataset is a comprehensive collection of 100,000 images specifically designed for autonomous driving applications. The dataset offers detailed detection annotations with 10 categories.

Sim10K. Sim10k [32] is a synthetic dataset comprising 10,000 rendered images simulated within the Grand Theft Auto gaming engine, specifically designed to facilitate the training and evaluation of object detection algorithms in autonomous driving systems.

VOC. VOC [17] is a general-purpose object detection dataset that includes bounding box and class annotations for common objects across 20 categories from the real world. Following [44], we combined the PASCAL VOC 2007 and 2012 editions, resulting in a total of 16,551 images.

Clipart. Clipart [30] dataset comprises 1,000 clipart images across the same 20 categories as the VOC dataset, exhibiting significant differences from real-world images. Following [44], we utilize 500 images each for training and testing purposes.

Comic. Comic [30] dataset consists of 2,000 comic-style images, featuring 6 categories shared with the VOC dataset. Following [31], we allocate 1,000 images each for training and testing.

Watercolor. Watercolor [30] dataset contains 2,000 images in a watercolor painting style, with 6 categories shared with the VOC dataset. Following [44], we use 1,000 images for both training and testing.

4.2 Cross-domian Detection Settings

Cross-Camera. We train on Cityscapes [13] (source domain) and validate on BDD100K [80] (target domain) to evaluate the cross-camera detection performance in diverse weather and scene conditions. We focus on the 7 same categories as SWDA [64].

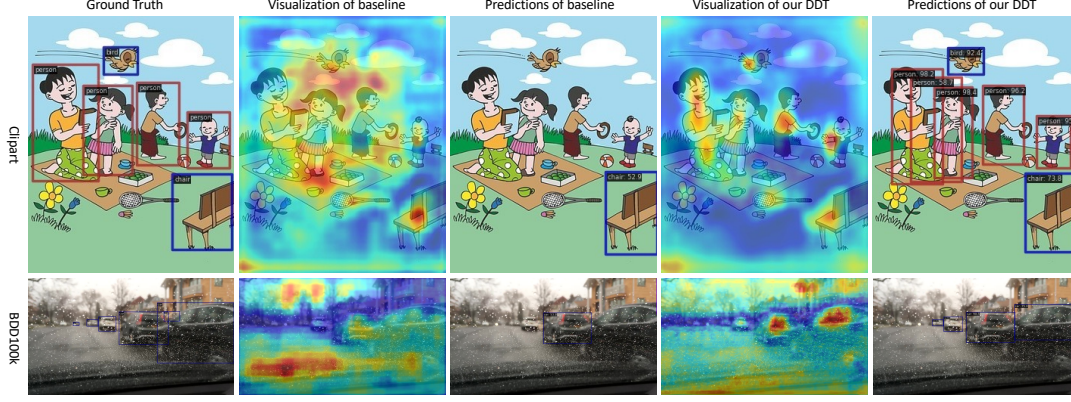


Figure 3: Qualitative prediction results and feature visualization of baseline and our DDT. Compared to the baseline, our method focuses more on specific classes of objects in the target domain images, effectively reducing the numbers of false negative on Clipart [13] (**first row**) and BDD100K [80] (**second row**).

Synthetic to Real (Syn2Real). We train on Sim10K (source domain) and validate on Cityscapes [13] and BDD100K [80] (target domain) to validate the performance of synthetic-to-real detection. Following SWDA [64], we focus on the shared category *car*.

Real to Artistic. We train on the VOC [17] (source domain) and perform validation on the Clipart [30], Comic [30], and Watercolor [30] (target domains) to assess cross-domain detection performance from real-world images to artistic styles. Referring to AT [44] and D-ADAPT [31], we respectively apply the 20, 6, and 6 shared categories between VOC and each of the Clipart, Comic, and Watercolor.

4.3 Implementation Details

Following [31, 44, 64], we use Faster R-CNN [58] as the default detector with a ResNet101 [23] backbone pretrained on ImageNet [62], implemented with MMDetection [9]. The training and testing sizes of images are set to (1333, 800) for Cityscapes, BDD100K, and Sim10K, and (1200, 600) for VOC, Clipart, Comic, and Watercolor. The models are trained with 20,000 steps on two 3090 GPUs, with a total batch size of 16. We employ the SGD optimizer with an initial learning rate of 0.02, following the default settings in MMDetection.

In self-training, we refer to the settings in [15, 44] to apply both weak and strong augmentation on the unlabeled target domain. We employ the EMA update parameter α of 0.999 for the mean teacher model updates and simply set the loss weight λ to 1. We train exclusively on the source domain for the first 12000 steps and then perform joint training on both the source and target domain for the remaining 8000 steps.

For evaluation, we report the Average Precision (AP) for each object category and the mean Average Precision (mAP) across all categories, with applying an Intersection over Union (IoU) threshold of 0.5.

4.4 Results and Comparisons

In this section, we present the evaluation result of our DDT framework along with other SOTA approaches. Current cross-domain object detection methods employ different detectors [48, 58, 72, 92],

Table 1: Quantitative results on adaptation from Cityscapes to BDD100K (Cs→B). The bold indicates the best results.

Method	Reference	Detector	bicycle	bus	car	motorcycle	person	rider	truck	mAP
DA-Faster [11]	<i>CVPR'18</i>	FRCNN-V16	22.4	18.0	44.2	14.2	28.9	27.4	19.1	24.9
SWDA [64]	<i>CVPR'19</i>	FRCNN-V16	23.1	20.7	44.8	15.2	29.5	29.9	20.2	26.2
SCDA [91]	<i>CVPR'19</i>	FRCNN-V16	23.2	19.6	44.4	14.8	29.3	29.2	20.3	25.8
CRDA [77]	<i>CVPR'20</i>	FRCNN-R101	25.5	20.6	45.8	14.9	32.8	29.3	22.7	27.4
SED [43]	<i>AAAI'21</i>	FRCNN-V16	25.0	23.4	50.4	18.9	32.4	32.6	20.6	29.0
TDD [24]	<i>CVPR'22</i>	FRCNN-V16	28.8	25.5	53.9	24.5	39.6	38.9	24.1	33.6
PT [10]	<i>ICML'22</i>	FRCNN-V16	28.8	33.8	52.7	23.0	40.5	39.9	25.8	34.9
EPM [27]	<i>ECCV'20</i>	FCOS-R101	20.1	19.1	55.8	14.5	39.6	26.8	18.8	27.8
SIGMA [41]	<i>CVPR'22</i>	FCOS-R50	26.3	23.6	64.1	17.9	46.9	29.6	20.2	32.7
SIGMA++ [42]	<i>TPAMI'23</i>	FRCNN-V16	27.1	26.3	65.6	17.8	47.5	30.4	21.1	33.7
NSA [89]	<i>ICCV'23</i>	FRCNN-V16	/	/	/	/	/	/	/	35.5
HT [15]	<i>CVPR'23</i>	FCOS-V16	38.0	30.6	63.5	28.2	53.4	40.4	27.4	40.2
Baseline	/	FRCNN-R18	23.8	13.0	51.8	17.0	42.5	27.4	15.7	27.3
DDT(Ours)	/	FRCNN-R18	36.8	27.0	64.9	25.8	55.3	39.2	27.3	39.5+12.2
Baseline	/	FRCNN-R50	24.8	16.5	53.9	15.4	45.3	27.6	18.2	28.8
DDT(Ours)	/	FRCNN-R50	39.0	31.6	65.9	30.2	57.7	39.8	28.6	41.8+13.0
Baseline	/	FRCNN-R101	25.9	18.4	48.8	17.2	41.1	29.8	21.7	29.0
DDT(Ours)	/	FRCNN-R101	40.3	32.3	66.7	31.8	59.1	41.6	31.8	43.4+14.4

which we refer to as FRCNN, FCOS, SSD, and DETR in our table. Furthermore, the backbones with varying depths, including ResNet-18, ResNet-50, ResNet-101 [23], and VGG-16 [66], are denoted as R18, R50, R101, and V16, respectively. To provide a comprehensive comparison, we report the results of our method with ResNet18, ResNet50, and ResNet101. The *baseline* refers to the results that only train on the source domain and test on the target domain.

Cross-camera adaptation. Tab. 1 presents the results of the Cross-camera settings. Our DDT method achieved the best performance with mAP 43.4 on the target domain, surpassing the previous SOTA method HT [15] by 3.2 mAP and outperforming other methods by a significant margin. Notably, AT [44] and HT [15] utilize self-training framework, have demonstrated substantial performance improvements by enhancing the quality of generated pseudo labels. Leveraging the powerful feature representation capability of the diffusion model and its exceptional performance on

Table 2: Quantitative results on adaptation from Sim10K to BDD100K (S→B). The bold indicates the best results.

Method	Reference	Detector	mAP(car)
SWDA [64]	<i>CVPR'19</i>	FRCNN-V16	42.9
CDN [68]	<i>ECCV'20</i>	FRCNN-V16	45.3
Baseline	/	FRCNN-R18	30.9
DDT(Ours)	/	FRCNN-R18	57.2+26.3
Baseline	/	FRCNN-R50	34.4
DDT(Ours)	/	FRCNN-R50	57.6+23.2
Baseline	/	FRCNN-R101	34.2
DDT(Ours)	/	FRCNN-R101	58.3+24.1

Table 3: Quantitative results on adaptation from Sim10K to Cityscapes (S→Cs). The bold indicates the best results.

Method	Reference	Detector	mAP(car)
SSAL [54]	<i>NeurIPS'22</i>	FCOS-R50	51.8
O2NET [19]	<i>ACMMM'22</i>	DDETR-R50	54.1
DDF [47]	<i>TMM'22</i>	FRCNN-R50	44.3
D-ADAPT [31]	<i>ICLR'22</i>	FRCNN-R50	51.9
SCAN [40]	<i>AAAI'22</i>	FCOS-V16	52.6
MTTrans [81]	<i>ECCV'22</i>	DDETR-R50	57.9
SIGMA [41]	<i>CVPR'22</i>	FCOS-R50	53.7
TDD [42]	<i>CVPR'22</i>	FRCNN-V16	53.4
MGA [88]	<i>CVPR'22</i>	FCOS-R101	54.1
OADA [79]	<i>ECCV'22</i>	FCOS-V16	59.2
SIGMA++ [42]	<i>TPAMI'23</i>	FCOS-V16	53.7
CIGAR [50]	<i>CVPR'23</i>	FCOS-V16	58.5
NSA [89]	<i>ICCV'23</i>	FRCNN-V16	56.3
HT [15]	<i>CVPR'23</i>	FRCNN-V16	65.5
Baseline	/	FRCNN-R18	42.9
DDT(Ours)	/	FRCNN-R18	62.3+19.4
Baseline	/	FRCNN-R50	43.0
DDT(Ours)	/	FRCNN-R50	62.7+19.7
Baseline	/	FRCNN-R101	43.4
DDT(Ours)	/	FRCNN-R101	64.0+20.6

diverse images, our DDT method achieve a remarkable enhancement in cross-camera detection.

Synthetic to Real adaptation. In Tab. 2, our method achieves improvements of 26.3, 23.3, and 24.2 mAP on BDD100K [80] compared with baseline, respectively, surpassing the results of previous algorithms SWDA [64] and CDN [68]. Similarly, our method obtains improvements of 19.4, 19.7, and 19.3 mAP on Cityscapes [13], respectively, surpassing all methods except HT [15] in Table 3. It can be observed that detectors for synthetic-to-real detection, due to the significant differences between synthetic and real-world images, does not perform well with source data only, while our method significantly improves the cross-domain performance from Sim10K [32] to BDD100K [80] and Cityscapes [13].

Real to Artistic adaptation. In Tab. 4, 5, and 6, we show the results of real to artistic cross-domain object detection. Our results

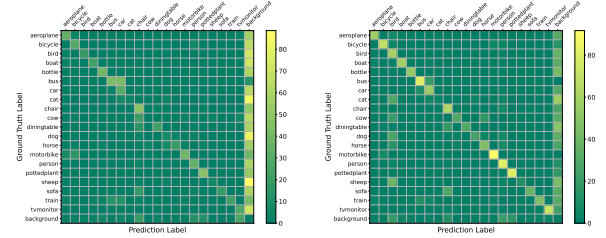
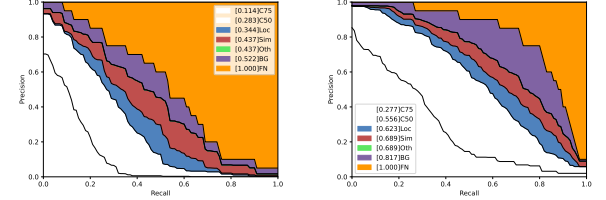
(a) Confusion matrix of **baseline** (left) and **DDT** (right)(b) COCO [46] style detection error analysis of the **baseline** (left) and **DDT** (right)

Figure 4: Error analysis on Clipart. It is evident that our method significantly reduces false negatives, which correspond to missed detections.

of Resnet50 and ResNet101 significantly surpass the previous best method AT [44] by 3.9 and 4.8 mAP, respectively. On Comic [30], the results of ResNet18, ResNet50, and ResNet101 [23] greatly surpass the previous best result of AT [44], by 2.0, 6.5, and 9.7 mAP, respectively. Similarly, our best result surpasses AT [44] by 3.8 mAP on Watercolor [30] as shown in Tab. 6. In real to artistic benchmark, overall, we find that due to the significant differences between real-world images and artistic-style images, the cross-domain performance is poor. Compared to the baseline, our method exhibits an average relative improvement of 95%, 163%, and 48% on Clipart, Comic, and Watercolor, respectively. This indicates that real to artistic adaptation is a challenging task, and it also demonstrates that our approach we have successfully improved the cross-domain performance by reducing the gap between real and artistic domain.

4.5 Ablation Studies

We conduct additional experiments to analyze the feature representation capabilities of different models. Specifically, we compared our diffusion model with powerful backbones, including ConvNext [52], Swin Transformer [51], ViT [16], as well as the self-supervised method MAE [22], pretrained on ImageNet [62]. Additionally, GLIP [36], which is pretrained on a larger dataset and has shown promising performance on object detection benchmarks. Our objective is to investigate two questions:

- (1) Will the diffusion model offer better intra-domain and cross-domain feature representation?
- (2) Will the diffusion model serve as a better teacher?

Ablation Study on the Intra-domain and Cross-domain Representation. To answer the first question, we evaluate the performance of seven models across different data settings in Tab. 7.

Table 4: Quantitative results on adaptation from VOC to Clipart ($V \rightarrow Ca$). The bold indicates the best results.

Method	Reference	Detector	aero	bicycle	bird	boat	bottle	bus	car	cat	chair	cow	table	dog	horse	bike	psn	plant	sheep	sofa	train	tv	mAP
AT [44]	<i>CVPR'22</i>	FRCNN-V16	33.8	60.9	38.6	49.4	52.4	53.9	56.7	7.5	52.8	63.5	34.0	25.0	62.2	72.1	77.2	57.7	27.2	52.0	55.7	54.1	49.3
D-ADAPT [31]	<i>ICLR'22</i>	FRCNN-R50	56.4	63.2	42.3	40.9	45.3	77.0	48.7	25.4	44.3	58.4	31.4	24.5	47.1	75.3	69.3	43.5	27.9	34.1	60.7	64.0	49.0
TIA [85]	<i>CVPR'22</i>	FRCNN-R101	42.2	66.0	36.9	37.3	43.7	71.8	49.7	18.2	44.9	58.9	18.2	29.1	40.7	87.8	67.4	49.7	27.4	27.8	57.1	50.6	46.3
LODS [38]	<i>CVPR'22</i>	FRCNN-R101	43.1	61.4	40.1	36.8	48.2	45.8	48.3	20.4	44.8	53.3	32.5	26.1	40.6	86.3	68.5	48.9	25.4	33.2	44.0	56.5	45.2
CIGAR [50]	<i>CVPR'23</i>	FCOS-R101	35.2	55.0	39.2	30.7	60.1	58.1	46.9	31.8	47.0	61.0	21.8	26.7	44.6	52.4	68.5	54.4	31.3	38.8	56.5	63.5	46.2
CMT [3]	<i>CVPR'23</i>	FRCNN-V16	39.8	56.3	38.7	39.7	60.4	35.0	56.0	7.1	60.1	60.4	35.8	28.1	67.8	84.5	80.1	55.5	20.3	32.8	42.3	38.2	47.0
Baseline	/	FRCNN-R18	25.0	36.4	16.2	19.6	34.3	50.7	30.3	0.2	33.6	5.5	22.1	6.5	23.3	47.9	36.1	26.8	3.2	18.5	31.7	25.1	24.6
DDT(Ours)			55.8	64.8	37.0	37.3	46.5	61.7	52.4	3.3	50.8	39.9	36.6	25.1	46.9	87.4	77.6	52.7	25.2	40.1	45.0	44.9	46.5+21.9
Baseline	/	FRCNN-R50	29.5	36.1	22.8	25.6	34.2	41.3	27.6	3.4	39.2	8.3	28.0	5.2	18.8	47.9	34.1	37.6	4.0	21.8	31.8	24.0	26.0
DDT(Ours)			48.9	64.9	41.1	48.1	60.5	76.6	60.2	7.9	57.4	51.5	40.8	33.0	55.4	98.0	82.8	60.1	35.2	36.0	50.8	55.8	53.2+27.2
Baseline	/	FRCNN-R101	36.7	27.2	22.6	22.8	38.5	46.4	32.2	10.7	40.7	7.2	27.2	7.6	28.2	56.1	38.2	38.2	9.2	29.3	25.9	21.6	28.3
DDT(Ours)			56.1	66.6	39.4	55.2	51.3	79.9	62.1	8.3	57.9	46.3	40.5	39.3	51.4	96.3	84.5	60.9	28.0	42.7	56.7	59.2	55.6+27.3

Table 5: Quantitative results on adaptation from VOC to Comic ($V \rightarrow Co$). The bold indicates the best results.

Method	Reference	Detector	bicycle	bird	car	cat	dog	person	mAP
DA-Faster [11]	<i>CVPR'18</i>	FRCNN-V16	31.1	10.3	15.5	12.4	19.3	39.0	21.2
SWDA [64]	<i>CVPR'19</i>	FRCNN-V16	36.4	21.8	29.8	15.1	23.5	49.6	29.4
STABR [33]	<i>CVPR'19</i>	SSD-V16	50.6	13.6	31.0	7.5	16.4	41.4	26.8
MCRA [86]	<i>ECCV'20</i>	FRCNN-V16	47.9	20.5	37.4	20.6	24.5	50.2	33.5
I3Net [8]	<i>CVPR'21</i>	SSD-V16	47.5	19.9	33.2	11.4	19.4	49.1	30.1
DBGL [5]	<i>ICCV'21</i>	FRCNN-R101	35.6	20.3	33.9	16.4	26.6	45.3	29.7
D-ADAPT [31]	<i>ICLR'22</i>	FRCNN-R101	52.4	25.4	42.3	43.7	25.7	53.5	40.5
Baseline	/	FRCNN-R18	29.4	6.8	11.6	5.6	7.4	26.3	14.5
DDT(Ours)			56.8	21.2	46.6	25.5	32.3	72.6	42.5+28.0
Baseline	/	FRCNN-R50	37.1	6.9	29.9	6.9	10.5	30.0	20.2
DDT(Ours)			60.9	28.2	52.5	29.3	36.8	74.5	47.0+26.8
Baseline	/	FRCNN-R101	37.0	6.8	31.2	4.8	7.2	26.8	19.0
DDT(Ours)			63.2	34.8	56.6	31.7	39.0	75.9	50.2+31.2

Table 6: Quantitative results on adaptation from VOC to Watercolor ($V \rightarrow W$). The bold indicates the best results.

Method	Reference	Detector	bicycle	bird	car	cat	dog	person	mAP
SWDA [11]	<i>CVPR'19</i>	FRCNN-V16	82.3	55.9	46.5	32.7	35.5	66.7	53.3
MCRA [87]	<i>ECCV'20</i>	FRCNN-V16	87.9	52.1	51.8	41.6	33.8	68.8	56.0
UMT [14]	<i>CVPR'21</i>	FRCNN-R101	88.2	55.3	51.7	39.8	43.6	69.9	58.1
I1OD [75]	<i>TPAMI'21</i>	FRCNN-V16	95.8	54.3	48.3	42.4	35.1	65.8	56.9
I3Net [8]	<i>CVPR'21</i>	SSD-V16	81.1	49.3	46.2	35.0	31.9	65.7	51.5
SADA [12]	<i>IJCV'21</i>	FRCNN-R50	82.9	54.6	52.3	40.5	37.7	68.2	56.0
CDG [37]	<i>AAAI'21</i>	FRCNN-V16	97.7	53.1	52.1	47.3	38.7	68.9	59.7
VDD [76]	<i>ICCV'21</i>	FRCNN-V16	90.0	56.6	49.2	39.5	38.8	65.3	56.6
DBGL [5]	<i>ICCV'21</i>	FRCNN-R101	83.1	49.3	50.6	39.8	38.7	61.3	53.8
AT [44]	<i>CVPR'22</i>	FRCNN-V16	93.6	56.1	58.9	37.3	39.6	73.8	59.9
LODS [38]	<i>CVPR'22</i>	FRCNN-R101	95.2	53.1	46.9	37.2	47.6	69.3	58.2
Baseline	/	FRCNN-R18	71.4	36.4	39.1	19.9	12.7	52.0	38.6
DDT(Ours)			81.9	53.7	54.3	37.7	31.5	68.3	54.6+16.0
Baseline	/	FRCNN-R50	68.2	40.2	44.7	21.7	10.3	44.0	38.2
DDT(Ours)			96.4	58.6	52.6	33.7	36.2	71.9	58.2+20.0
Baseline	/	FRCNN-R101	72.5	40.1	45.7	30.5	18.1	45.8	42.1
DDT(Ours)			87.1	64.0	55.7	50.6	48.8	75.7	63.7+21.6

Table 7: Results of our diffusion feature extractor (Diff.) compared to other backbones. The bold and underlined represent the best and second performances, respectively

Backbones	$V \rightarrow V$	$Ca \rightarrow Ca$	$V \rightarrow Ca$	Rel.(%)	$S \rightarrow S$	$Cs \rightarrow Cs$	$S \rightarrow Cs$	Rel.(%)	$B \rightarrow B$	$S \rightarrow B$	Rel.(%)
R101 [23]	84.0	40.0	28.3	70.8	83.0	72.6	43.4	59.8	74.2	34.2	46.1
ConvNext-Base [52]	91.5	62.8	<u>44.1</u>	70.2	87.9	78.2	61.8	<u>79.0</u>	80.5	44.8	55.6
Swin-Base [51]	86.9	51.6	32.2	62.4	<u>87.6</u>	73.7	53.7	72.8	79.7	39.3	49.4
VIT-Base [16]	84.9	31.5	28.6	<u>90.8</u>	77.6	72.1	48.4	67.1	73.4	40.9	55.7
MAE (VIT-Base) [16, 22]	85.8	37.8	26.4	69.8	85.0	<u>77.7</u>	57.9	74.5	78.3	40.9	52.2
GLIP (Swin-Tiny) [36, 51]	<u>88.1</u>	<u>55.6</u>	39.8	71.6	86.5	77.2	59.3	76.8	<u>79.7</u>	50.4	63.3
Diff (Ours)	75.4	43.9	47.4	108.1	76.1	71.7	58.2	81.2	71.8	<u>50.1</u>	69.8

Table 8: Results of using our diffusion backbone (Diff.) as the teacher model to train student models on different backbones. The bold indicates the best results.

Detector Setting		Cross Domain Settings		
Student	Teacher	$V \rightarrow Ca$	$S \rightarrow Cs$	$S \rightarrow B$
R101 [23]	ConvNext-Base [52]	43.2+19.9	60.2+16.8	54.6+20.4
R101 [23]	Swin-Base [51]	35.1+6.8	57.5+14.1	52.9+18.7
R101 [23]	VIT-Base [16]	37.4+9.1	54.8+11.4	51.1+16.9
R101 [23]	MAE (VIT-Base) [16, 22]	35.8+7.5	59.0+16.2	53.2+19.0
R101 [23]	GLIP (Swin-Tiny) [36, 51]	39.6+11.3	58.9+15.5	54.0+19.8
R101 [23]	Diff. (Ours)	55.6+27.3	64.0+20.6	58.3+24.1
ConvNext-Base [52]	Diff. (Ours)	59.5+18.4	63.5+1.7	59.6+7.1
Swin-Base [51]	Diff. (Ours)	46.6+14.4	63.6+9.9	58.6+13.8
VIT-Base [16]	Diff. (Ours)	41.7+13.1	60.2+11.8	54.9+15.6
MAE (VIT-Base) [16, 22]	Diff. (Ours)	43.1+16.7	64.6+6.7	57.3+16.4
GLIP (Swin-Tiny) [36, 51]	Diff. (Ours)	49.5+9.7	64.0+4.7	59.5+9.4

Table 9: Results of ablation experiments on Diffusion Teacher and Mean Teacher.

Settings of Self-training	$Cs \rightarrow B$	$S \rightarrow Cs$	$S \rightarrow B$	$V \rightarrow Ca$	$V \rightarrow Co$	$V \rightarrow W$
DDT (R101)	43.4	64.0	58.3	55.6	50.2	63.7
w/o Mean Teacher	40.6-2.8	62.5-1.5	55.5-2.8	49.1-6.5	46.2-4.0	61.0-2.7
w/o Diffusion Teacher	40.1-3.3	57.4-6.6	54.4-3.9	46.9-8.7	37.5-12.7	57.4-6.3
w/o All Teacher	37.5-5.9	56.1-7.9	53.7-4.6	41.9-13.7	37.4-12.8	57.1-6.6

Table 10: Ablation results of the diffusion backbone under different time steps and save steps.

Time Steps	Save Steps	Train Time (s/iter)	Inf. Time (ms/image)	Cs→B	S→Cs	S→B	V→Ca	V→Co	V→W
1	1	0.82	271.1	29.8	57.2	50.4	37.8	36.9	52.7
2	2	1.14	402.5	31.0	57.5	50.1	39.3	36.3	51.8
<u>5</u>	<u>5</u>	1.56	780.4	32.7	58.2	50.1	47.4	39.4	53.8
10	5	2.84	1424.2	29.8	56.3	51.1	48.4	40.9	53.7
20	10	5.48	2710.2	28.0	55.2	50.2	48.8	41.3	54.6

Specifically, we compared their intra-domain performance in training and testing within the source domain ($V \rightarrow V$, $S \rightarrow S$) and target domain ($Ca \rightarrow Ca$, $Cs \rightarrow Cs$, $B \rightarrow B$), and cross-domain testing ($V \rightarrow Ca$, $S \rightarrow Cs$, $S \rightarrow B$) to assess their cross-domain feature representation capabilities. we find that our diffusion model performs poorly within the intra-domain, lagging behind the other six models. In cross-domain testing, our diffusion model outperformed other methods on Clipart [30] but remained inferior to ConvNext [52] and GLIP [36]. Additionally, we calculate the cross-domain metrics for each model and the results obtained from training and testing in the target domain to measure the relative cross-domain capabilities of each models, represented as "Rel." in Tab. 7. We find that the diffusion model consistently achieves the best relative cross-domain performance. Overall, the answer to the first question may be disappointing, as the diffusion detector shows some improvement in cross-domain performance but still fall behind the detectors with stronger and large-dataset pretrained backbones.

Ablation Study of Different Teachers. In Tab. 8, we present the performance of different teacher and student settings for cross-domain detection. First, we use ResNet101 [23] as the student and other models as teacher. We find that although the diffusion model performs worse than ConvNext [52] and GLIP [36] in cross-domain performance, it exhibits significantly better performance when used as a teacher model. Furthermore, when we use the diffusion model as the teacher and the other six models as students, it consistently brings large improvements. This answers our second question, confirming that our diffusion model is indeed a better teacher, even when faced with highly competent students and consistently improve their performance.

Ablation Results on Diffusion and Mean Teacher. To better understand the significance of teachers in our DDT, we present the results of different teacher model settings in Tab. 9. The findings reveal that excluding the Mean Teacher and Diffusion Teacher from our method leads to an average decrease of 3.1 and 6.7 mAP, respectively. When all teachers are removed, the self-training performance experiences an average decline of 8.3 mAP. These results clearly demonstrate that both the diffusion teacher and mean teacher play crucial roles in our DDT and are indispensable for achieving better performance. Fig. 1 provides an intuitive illustration of the impacts of the diffusion teacher and mean teacher in training process.

Ablation Results of Different Diffusion Settings. We report the results of the diffusion models with different time steps and save steps settings in Tab. 10. It is observed that in cross-domain detection with a larger domain gap (real to artistic), longer time

steps and save steps show better results. We consider a trade-off between accuracy and efficiency and choose time steps 5 and save steps 5 as our default settings.

4.6 Analysis

Analysis of Feature Representation of Diffusion Model. The results in Tab. 7 and 8 further deepen our understanding of the feature representation of diffusion model and its advantages in cross-domain detection. In our view, the observed results can be attributed as: fully frozen weight and adaptation of the diffusion model with the light structure that aligns with the hierarchical feature outputs, limit its performance within the intro-domain compared to fully trainable models. However, when applied as a teacher, the diffusion model guides the student to achieve superior performance in cross-domain, surpassing even the teacher itself. We think that the improved cross-domain representation ability can be attributed to the inherent characteristics of the diffusion model as well as the advantages gained from supervised learning on the source domain. In contrast, other fully trainable teacher models often concentrate primarily on supervised learning on the source domain, resulting in homogeneous optimization and limited guidance for the student. As a result, it becomes challenging to enhance the performance of the students to the level achieved by the homogeneous teacher. These results provide compelling evidence for the advantages of the diffusion model in addressing cross-domain detection tasks.

Error analysis. Error analysis on Clipart [30] reveals that false negatives, i.e., missed detections, are the main factor impacting the performance on the target domain as shown in Fig. 4. Our method significantly reduces the number of missed detections, thereby greatly improving the performance of cross-domain detection. A representation of prediction results and feature visualization further corroborate this conclusion, as depicted in the Fig. 3.

5 Conclusion

In this paper, we propose a domain adaptive method based on the diffusion model to address the performance degradation caused by the large gap between the source and target domain. We employ a frozen-weight diffusion model as the backbone and extract intermediate feature in the inversion process for the detection task, which we refer to as the diffusion teacher. Subsequently, we apply diffusion teacher in the self-training framework to generate pseudo labels on the unlabeled target domain, guiding the learning of the student model. Our method significantly improves cross-domain detection performance on six datasets, achieving an average improvement of 21.2% mAP compared to the baseline, surpassing the current SOTA methods by an average of 5.7% mAP, without compromising the inference speed. Furthermore, we validate the consistent performance improvement of our method in more extensive experiments for detectors with more powerful backbones, demonstrating the strong and universality domain adaptive capability of our approach.

6 Acknowledgment

The authors would like to thank Xiamen University and Unmanned Aerial Vehicle (UAV) Laboratory for the funding and providing with all the necessary technical support.

References

- [1] Dmitry Baranchuk, Andrey Voynov, Ivan Rubachev, Valentin Khulkov, and Artem Babenko. 2022. Label-Efficient Semantic Segmentation with Diffusion Models. In *International Conference on Learning Representations*.
- [2] Zhaowei Cai and Nuno Vasconcelos. 2018. Cascade r-cnn: Delving into high quality object detection. In *Proceedings of the IEEE conference on computer vision and pattern recognition*. 6154–6162.
- [3] Shengcao Cao, Dhiraj Joshi, Liang-Yan Gui, and Yu-Xiong Wang. 2023. Contrastive mean teacher for domain adaptive object detectors. In *Proceedings of the IEEE/CVF Conference on Computer Vision and Pattern Recognition*. 23839–23848.
- [4] Nicolas Carion, Francisco Massa, Gabriel Synnaeve, Nicolas Usunier, Alexander Kirillov, and Sergey Zagoruyko. 2020. End-to-end object detection with transformers. In *European conference on computer vision*. Springer, 213–229.
- [5] Chaoqi Chen, Jiongcheng Li, Zebiao Zheng, Yue Huang, Xinghao Ding, and Yizhou Yu. 2021. Dual bipartite graph learning: A general approach for domain adaptive object detection. In *Proceedings of the IEEE/CVF International Conference on Computer Vision*. 2703–2712.
- [6] Chaoqi Chen, Zebiao Zheng, Xinghao Ding, Yue Huang, and Qi Dou. 2020. Harmonizing transferability and discriminability for adapting object detectors. In *Proceedings of the IEEE/CVF conference on computer vision and pattern recognition*. 8869–8878.
- [7] Chaoqi Chen, Zebiao Zheng, Xinghao Ding, Yue Huang, and Qi Dou. 2020. Harmonizing transferability and discriminability for adapting object detectors. In *Proceedings of the IEEE/CVF conference on computer vision and pattern recognition*. 8869–8878.
- [8] Chaoqi Chen, Zebiao Zheng, Yue Huang, Xinghao Ding, and Yizhou Yu. 2021. I3net: Implicit instance-invariant network for adapting one-stage object detectors. In *Proceedings of the IEEE/CVF conference on computer vision and pattern recognition*. 12576–12585.
- [9] Kai Chen, Jiaqi Wang, Jiangmiao Pang, Yuhang Cao, Yu Xiong, Xiaoxiao Li, Shuyang Sun, Wansen Feng, Ziwei Liu, Jiarui Xu, et al. 2019. MMDetection: Open mmlab detection toolbox and benchmark. *arXiv preprint arXiv:1906.07155* (2019).
- [10] Meilin Chen, Weijie Chen, Shicai Yang, Jie Song, Xinchao Wang, Lei Zhang, Yunfeng Yan, Donglian Qi, Yueting Zhuang, Di Xie, et al. 2022. Learning Domain Adaptive Object Detection with Probabilistic Teacher. In *International Conference on Machine Learning*. PMLR, 3040–3055.
- [11] Yuhua Chen, Wen Li, Christos Sakaridis, Dengxin Dai, and Luc Van Gool. 2018. Domain adaptive faster r-cnn for object detection in the wild. In *Proceedings of the IEEE conference on computer vision and pattern recognition*. 3339–3348.
- [12] Yuhua Chen, Haoran Wang, Wen Li, Christos Sakaridis, Dengxin Dai, and Luc Van Gool. 2021. Scale-aware domain adaptive faster r-cnn. *International Journal of Computer Vision* 129, 7 (2021), 2223–2243.
- [13] Marius Cordts, Mohamed Omran, Sebastian Ramos, Timo Rehfeld, Markus Enzweiler, Rodrigo Benenson, Uwe Franke, Stefan Roth, and Bernt Schiele. 2016. The cityscapes dataset for semantic urban scene understanding. In *Proceedings of the IEEE conference on computer vision and pattern recognition*. 3213–3223.
- [14] Jinhong Deng, Wen Li, Yuhua Chen, and Lixin Duan. 2021. Unbiased mean teacher for cross-domain object detection. In *Proceedings of the IEEE/CVF Conference on Computer Vision and Pattern Recognition*. 4091–4101.
- [15] Jinhong Deng, Dongli Xu, Wen Li, and Lixin Duan. 2023. Harmonious teacher for cross-domain object detection. In *Proceedings of the IEEE/CVF Conference on Computer Vision and Pattern Recognition*. 23829–23838.
- [16] Alexey Dosovitskiy, Lucas Beyer, Alexander Kolesnikov, Dirk Weissenborn, Xiuhua Zhai, Thomas Unterthiner, Mostafa Dehghani, Matthias Minderer, Georg Heigold, Sylvain Gelly, et al. 2020. An image is worth 16x16 words: Transformers for image recognition at scale. *arXiv preprint arXiv:2010.11929* (2020).
- [17] Mark Everingham, Luc Van Gool, Christopher KI Williams, John Winn, and Andrew Zisserman. 2010. The pascal visual object classes (voc) challenge. *International journal of computer vision* 88 (2010), 303–338.
- [18] Yaroslav Ganin, Evgeniya Ustinova, Hana Ajakan, Pascal Germain, Hugo Larochelle, François Laviolette, Mario March, and Victor Lempitsky. 2016. Domain-adversarial training of neural networks. *Journal of machine learning research* 17, 59 (2016), 1–35.
- [19] Kaixiong Gong, Shuang Li, Shugang Li, Rui Zhang, Chi Harold Liu, and Qiang Chen. 2022. Improving transferability for domain adaptive detection transformers. In *Proceedings of the 30th ACM International Conference on Multimedia*. 1543–1551.
- [20] Ian Goodfellow, Jean Pouget-Abadie, Mehdi Mirza, Bing Xu, David Warde-Farley, Sherjil Ozair, Aaron Courville, and Yoshua Bengio. 2020. Generative adversarial networks. *Commun. ACM* 63, 11 (2020), 139–144.
- [21] Dayan Guan, Jiaxing Huang, Aoran Xiao, Shijian Lu, and Yanpeng Cao. 2021. Uncertainty-aware unsupervised domain adaptation in object detection. *IEEE Transactions on Multimedia* 24 (2021), 2502–2514.
- [22] Kaiming He, Xinlei Chen, Saining Xie, Yanghao Li, Piotr Dollár, and Ross Girshick. 2022. Masked autoencoders are scalable vision learners. In *Proceedings of the IEEE/CVF conference on computer vision and pattern recognition*. 16000–16009.
- [23] Kaiming He, Xiangyu Zhang, Shaoqing Ren, and Jian Sun. 2016. Deep residual learning for image recognition. In *Proceedings of the IEEE conference on computer vision and pattern recognition*. 770–778.
- [24] Mengzhe He, Yali Wang, Jiaxi Wu, Yiru Wang, Hanqing Li, Bo Li, Weihao Gan, Wei Wu, and Yu Qiao. 2022. Cross domain object detection by target-perceived dual branch distillation. In *Proceedings of the IEEE/CVF Conference on Computer Vision and Pattern Recognition*. 9570–9580.
- [25] Jonathan Ho, Ajay Jain, and Pieter Abbeel. 2020. Denoising diffusion probabilistic models. *Advances in neural information processing systems* 33 (2020), 6840–6851.
- [26] Lukas Hoyer, Dengxin Dai, Haoran Wang, and Luc Van Gool. 2023. MIC: Masked image consistency for context-enhanced domain adaptation. In *Proceedings of the IEEE/CVF conference on computer vision and pattern recognition*. 11721–11732.
- [27] Cheng-Chun Hsu, Yi-Hsuan Tsai, Yen-Yu Lin, and Ming-Hsuan Yang. 2020. Every pixel matters: Center-aware feature alignment for domain adaptive object detector. In *Computer Vision—ECCV 2020: 16th European Conference, Glasgow, UK, August 23–28, 2020, Proceedings, Part IX* 16. Springer, 733–748.
- [28] Han-Kai Hsu, Chun-Han Yao, Yi-Hsuan Tsai, Wei-Chih Hung, Hung-Yu Tseng, Maneesh Singh, and Ming-Hsuan Yang. 2020. Progressive domain adaptation for object detection. In *Proceedings of the IEEE/CVF winter conference on applications of computer vision*. 749–757.
- [29] Edward J Hu, Phillip Wallis, Zeyuan Allen-Zhu, Yuanzhi Li, Shean Wang, Lu Wang, Weizhu Chen, et al. 2022. LoRA: Low-Rank Adaptation of Large Language Models. In *International Conference on Learning Representations*.
- [30] Naoto Inoue, Ryosuke Furuta, Toshihiko Yamasaki, and Kiyoharu Aizawa. 2018. Cross-domain weakly-supervised object detection through progressive domain adaptation. In *Proceedings of the IEEE conference on computer vision and pattern recognition*. 5001–5009.
- [31] Junguang Jiang, Baixu Chen, Jianmin Wang, and Mingsheng Long. 2021. Decoupled Adaptation for Cross-Domain Object Detection. In *International Conference on Learning Representations*.
- [32] Matthew Johnson-Roberson, Charles Barto, Rounak Mehta, Sharath Nittur Sridhar, Karl Rosaen, and Ram Vasudevan. 2017. Driving in the Matrix: Can virtual worlds replace human-generated annotations for real world tasks?. In *2017 IEEE International Conference on Robotics and Automation (ICRA)*. IEEE.
- [33] Seunghyeon Kim, Jaehoon Choi, Taekyung Kim, and Changick Kim. 2019. Self-training and adversarial background regularization for unsupervised domain adaptive one-stage object detection. In *Proceedings of the IEEE/CVF International Conference on Computer Vision*. 6092–6101.
- [34] Taekyung Kim, Minki Jeong, Seunghyeon Kim, Seokwon Choi, and Changick Kim. 2019. Diversify and match: A domain adaptive representation learning paradigm for object detection. In *Proceedings of the IEEE/CVF Conference on Computer Vision and Pattern Recognition*. 12456–12465.
- [35] Congcong Li, Dawei Du, Libo Zhang, Longyin Wen, Tiejian Luo, Yanjun Wu, and Pengfei Zhu. 2020. Spatial Attention Pyramid Network for Unsupervised Domain Adaptation. In *European Conference on Computer Vision*. 481–497.
- [36] Liunan Harold Li, Pengchuan Zhang, Haotian Zhang, Jianwei Yang, Chunyuan Li, Yiyu Zhong, Lijuan Wang, Lu Yuan, Lei Zhang, Jenq-Neng Hwang, et al. 2022. Grounded language-image pre-training. In *Proceedings of the IEEE/CVF Conference on Computer Vision and Pattern Recognition*. 10965–10975.
- [37] Shuai Li, Jianqiang Huang, Xian-Sheng Hua, and Lei Zhang. 2021. Category dictionary guided unsupervised domain adaptation for object detection. In *Proceedings of the AAAI conference on artificial intelligence*, Vol. 35. 1949–1957.
- [38] Shuaifeng Li, Mao Ye, Xiatian Zhu, Lihua Zhou, and Lin Xiong. 2022. Source-free object detection by learning to overlook domain style. In *Proceedings of the IEEE/CVF Conference on Computer Vision and Pattern Recognition*. 8014–8023.
- [39] Wuyang Li, Xinyu Liu, Xiwen Yao, and Yixuan Yuan. 2022. Scan: Cross domain object detection with semantic conditioned adaptation. In *Proceedings of the AAAI Conference on Artificial Intelligence*, Vol. 36. 1421–1428.
- [40] Wuyang Li, Xinyu Liu, Xiwen Yao, and Yixuan Yuan. 2022. Scan: Cross domain object detection with semantic conditioned adaptation. In *Proceedings of the AAAI Conference on Artificial Intelligence*, Vol. 36. 1421–1428.
- [41] Wuyang Li, Xinyu Liu, and Yixuan Yuan. 2022. Sigma: Semantic-complete graph matching for domain adaptive object detection. In *Proceedings of the IEEE/CVF Conference on Computer Vision and Pattern Recognition*. 5291–5300.
- [42] Wuyang Li, Xinyu Liu, and Yixuan Yuan. 2023. Sigma++: Improved semantic-complete graph matching for domain adaptive object detection. *IEEE Transactions on Pattern Analysis and Machine Intelligence* (2023).
- [43] Xianfeng Li, Weijie Chen, Di Xie, Shicai Yang, Peng Yuan, Shiliang Pu, and Yueting Zhuang. 2021. A free lunch for unsupervised domain adaptive object detection without source data. In *Proceedings of the AAAI Conference on Artificial Intelligence*, Vol. 35. 8474–8481.
- [44] Yu-Jhe Li, Xiaoliang Dai, Chih-Yao Ma, Yen-Cheng Liu, Kan Chen, Bichen Wu, Zijian He, Kris Kitani, and Peter Vajda. 2022. Cross-domain adaptive teacher for object detection. In *Proceedings of the IEEE/CVF Conference on Computer Vision and Pattern Recognition*. 7581–7590.
- [45] Tsung-Yi Lin, Priya Goyal, Ross Girshick, Kaiming He, and Piotr Dollár. 2017. Focal loss for dense object detection. In *Proceedings of the IEEE international conference on computer vision*. 2980–2988.

- [46] Tsung-Yi Lin, Michael Maire, Serge Belongie, James Hays, Pietro Perona, Deva Ramanan, Piotr Dollár, and C Lawrence Zitnick. 2014. Microsoft coco: Common objects in context. In *Computer Vision—ECCV 2014: 13th European Conference, Zurich, Switzerland, September 6–12, 2014, Proceedings, Part V 13*. Springer, 740–755.
- [47] Dongnan Liu, Chaoyi Zhang, Yang Song, Heng Huang, Chenyu Wang, Michael Barnett, and Weidong Cai. 2022. Decompose to adapt: Cross-domain object detection via feature disentanglement. *IEEE Transactions on Multimedia* 25 (2022), 1333–1344.
- [48] Wei Liu, Dragomir Anguelov, Dumitru Erhan, Christian Szegedy, Scott Reed, Cheng-Yang Fu, and Alexander C Berg. 2016. Ssd: Single shot multibox detector. In *Computer Vision—ECCV 2016: 14th European Conference, Amsterdam, The Netherlands, October 11–14, 2016, Proceedings, Part I 14*. Springer, 21–37.
- [49] Xinyu Liu, Wuyang Li, Qiushi Yang, Baopu Li, and Yixuan Yuan. 2022. Towards robust adaptive object detection under noisy annotations. In *Proceedings of the IEEE/CVF conference on computer vision and pattern recognition*. 14207–14216.
- [50] Yabo Liu, Jinghua Wang, Chao Huang, Yaowei Wang, and Yong Xu. 2023. CIGAR: Cross-Modality Graph Reasoning for Domain Adaptive Object Detection. In *Proceedings of the IEEE/CVF Conference on Computer Vision and Pattern Recognition*. 23776–23786.
- [51] Ze Liu, Yutong Lin, Yue Cao, Han Hu, Yixuan Wei, Zheng Zhang, Stephen Lin, and Baining Guo. 2021. Swin transformer: Hierarchical vision transformer using shifted windows. In *Proceedings of the IEEE/CVF international conference on computer vision*. 10012–10022.
- [52] Zhuang Liu, Hanzi Mao, Chao-Yuan Wu, Christoph Feichtenhofer, Trevor Darrell, and Saining Xie. 2022. A convnet for the 2020s. In *Proceedings of the IEEE/CVF conference on computer vision and pattern recognition*. 11976–11986.
- [53] Grace Luo, Lisa Dunlap, Dong Huk Park, Aleksander Holynski, and Trevor Darrell. 2024. Diffusion hyperfeatures: Searching through time and space for semantic correspondence. *Advances in Neural Information Processing Systems* 36 (2024).
- [54] Muhammad Akhtar Munir, Muhammad Haris Khan, M Sarfraz, and Mohsen Ali. 2021. Ssal: Synergizing between self-training and adversarial learning for domain adaptive object detection. *Advances in Neural Information Processing Systems* 34 (2021), 22770–22782.
- [55] Siyuan Qiao, Liang-Chieh Chen, and Alan Yuille. 2021. Detectors: Detecting objects with recursive feature pyramid and switchable atrous convolution. In *Proceedings of the IEEE/CVF conference on computer vision and pattern recognition*. 10213–10224.
- [56] Aditya Ramesh, Mikhail Pavlov, Gabriel Goh, Scott Gray, Chelsea Voss, Alec Radford, Mark Chen, and Ilya Sutskever. 2021. Zero-shot text-to-image generation. In *International conference on machine learning*. Pmlr, 8821–8831.
- [57] Joseph Redmon and Ali Farhadi. 2018. Yolov3: An incremental improvement. *arXiv preprint arXiv:1804.02767* (2018).
- [58] Shaoqing Ren, Kaiming He, Ross Girshick, and Jian Sun. 2016. Faster R-CNN: Towards real-time object detection with region proposal networks. *IEEE transactions on pattern analysis and machine intelligence* 39, 6 (2016), 1137–1149.
- [59] Robin Rombach, Andreas Blattmann, Dominik Lorenz, Patrick Esser, and Björn Ommer. 2022. High-resolution image synthesis with latent diffusion models. In *Proceedings of the IEEE/CVF conference on computer vision and pattern recognition*. 10684–10695.
- [60] Olaf Ronneberger, Philipp Fischer, and Thomas Brox. 2015. U-net: Convolutional networks for biomedical image segmentation. In *Medical image computing and computer-assisted intervention—MICCAI 2015: 18th international conference, Munich, Germany, October 5–9, 2015, proceedings, part III 18*. Springer, 234–241.
- [61] Aruni RoyChowdhury, Prithvijit Chakrabarty, Ashish Singh, SouYoung Jin, Huaizu Jiang, Liangliang Cao, and Erik Learned-Miller. 2019. Automatic adaptation of object detectors to new domains using self-training. In *Proceedings of the IEEE/CVF Conference on Computer Vision and Pattern Recognition*. 780–790.
- [62] Olga Russakovsky, Jia Deng, Hao Su, Jonathan Krause, Sanjeev Satheesh, Sean Ma, Zhiheng Huang, Andrej Karpathy, Aditya Khosla, Michael Bernstein, et al. 2015. Imagenet large scale visual recognition challenge. *International journal of computer vision* 115 (2015), 211–252.
- [63] Chitwan Saharia, William Chan, Saurabh Saxena, Lala Li, Jay Whang, Emily L Denton, Kamyar Ghasemipour, Raphael Gontijo Lopes, Burcu Karagol Ayan, Tim Salimans, et al. 2022. Photorealistic text-to-image diffusion models with deep language understanding. *Advances in neural information processing systems* 35 (2022), 36479–36494.
- [64] Kuniaki Saito, Yoshitaka Ushiku, Tatsuya Harada, and Kate Saenko. 2019. Strong-weak distribution alignment for adaptive object detection. In *Proceedings of the IEEE/CVF conference on computer vision and pattern recognition*. 6956–6965.
- [65] Christos Sakaridis, Dengxin Dai, and Luc Van Gool. 2018. Semantic foggy scene understanding with synthetic data. *International Journal of Computer Vision* 126 (2018), 973–992.
- [66] Karen Simonyan and Andrew Zisserman. 2014. Very deep convolutional networks for large-scale image recognition. *arXiv preprint arXiv:1409.1556* (2014).
- [67] Jiaming Song, Chenlin Meng, and Stefano Ermon. 2020. Denoising diffusion implicit models. *arXiv preprint arXiv:2010.02502* (2020).
- [68] Peng Su, Kun Wang, Xingyu Zeng, Shixiang Tang, Dapeng Chen, Di Qiu, and Xiaogang Wang. 2020. Adapting object detectors with conditional domain normalization. In *Computer Vision—ECCV 2020: 16th European Conference, Glasgow, UK, August 23–28, 2020, Proceedings, Part XI 16*. Springer, 403–419.
- [69] Luming Tang, Menglin Jia, Qianqian Wang, Cheng Perng Phoo, and Bharath Hariharan. 2023. Emergent correspondence from image diffusion. *Advances in Neural Information Processing Systems* 36 (2023), 1363–1389.
- [70] Renshuai Tao, Hainan Li, Tianbo Wang, Yanlu Wei, Yifu Ding, Bowei Jin, Hongping Zhi, Xianglong Liu, and Aishan Liu. 2022. Exploring endogenous shift for cross-domain detection: A large-scale benchmark and perturbation suppression network. In *2022 IEEE/CVF Conference on Computer Vision and Pattern Recognition (CVPR)*. IEEE, 21157–21167.
- [71] Antti Tarvainen and Harri Valpola. 2017. Mean teachers are better role models: Weight-averaged consistency targets improve semi-supervised deep learning results. *Advances in neural information processing systems* 30 (2017).
- [72] Zhi Tian, Chunhua Shen, Hao Chen, and Tong He. 2020. FCOS: A simple and strong anchor-free object detector. *IEEE Transactions on Pattern Analysis and Machine Intelligence* 44, 4 (2020), 1922–1933.
- [73] Narek Tumanyan, Michal Geyer, Shai Bagon, and Tali Dekel. 2023. Plug-and-play diffusion features for text-driven image-to-image translation. In *Proceedings of the IEEE/CVF Conference on Computer Vision and Pattern Recognition*. 1921–1930.
- [74] Chien-Yao Wang, Alexey Bochkovskiy, and Hong-Yuan Mark Liao. 2023. YOLOv7: Trainable bag-of-freebies sets new state-of-the-art for real-time object detectors. In *Proceedings of the IEEE/CVF conference on computer vision and pattern recognition*. 7464–7475.
- [75] Aming Wu, Yahong Han, Linchao Zhu, and Yi Yang. 2021. Instance-invariant domain adaptive object detection via progressive disentanglement. *IEEE Transactions on Pattern Analysis and Machine Intelligence* 44, 8 (2021), 4178–4193.
- [76] Aming Wu, Rui Liu, Yahong Han, Linchao Zhu, and Yi Yang. 2021. Vector-decomposed disentanglement for domain-invariant object detection. In *Proceedings of the IEEE/CVF International Conference on Computer Vision*. 9342–9351.
- [77] Chang-Dong Xu, Xing-Ran Zhao, Xin Jin, and Xiu-Shen Wei. 2020. Exploring categorical regularization for domain adaptive object detection. In *Proceedings of the IEEE/CVF Conference on Computer Vision and Pattern Recognition*. 11724–11733.
- [78] Jiarui Xu, Sifei Liu, Arash Vahdat, Wonmin Byeon, Xiaolong Wang, and Shalini De Mello. 2023. Open-vocabulary panoptic segmentation with text-to-image diffusion models. In *Proceedings of the IEEE/CVF Conference on Computer Vision and Pattern Recognition*. 2955–2966.
- [79] Jayeon Yoo, Inseop Chung, and Nojun Kwak. 2022. Unsupervised domain adaptation for one-stage object detector using offsets to bounding box. In *European Conference on Computer Vision*. Springer, 691–708.
- [80] Fisher Yu, Haofeng Chen, Xin Wang, Wenqi Xian, Yingying Chen, Fangchen Liu, Vashisht Madhavan, and Trevor Darrell. 2020. Bdd100k: A diverse driving dataset for heterogeneous multitask learning. In *Proceedings of the IEEE/CVF conference on computer vision and pattern recognition*. 2636–2645.
- [81] Jinze Yu, Jiaming Liu, Xiaobao Wei, Haoyi Zhou, Yohei Nakata, Denis Gudovskiy, Tomoyuki Okuno, Jianxin Li, Kurt Keutzer, and Shanghang Zhang. 2022. MT-Trans: Cross-domain object detection with mean teacher transformer. In *European Conference on Computer Vision*. Springer, 629–645.
- [82] Hao Zhang, Feng Li, Shilong Liu, Lei Zhang, Hang Su, Jun Zhu, Lionel Ni, and Heung-Yeung Shum. 2022. DINO: DETR with Improved DeNoising Anchor Boxes for End-to-End Object Detection. In *The Eleventh International Conference on Learning Representations*.
- [83] Lvmin Zhang, Anyi Rao, and Maneesh Agrawala. 2023. Adding conditional control to text-to-image diffusion models. In *Proceedings of the IEEE/CVF International Conference on Computer Vision*. 3836–3847.
- [84] Shifeng Zhang, Cheng Chi, Yongqiang Yao, Zhen Lei, and Stan Z Li. 2020. Bridging the gap between anchor-based and anchor-free detection via adaptive training sample selection. In *Proceedings of the IEEE/CVF conference on computer vision and pattern recognition*. 9759–9768.
- [85] Liang Zhao and Limin Wang. 2022. Task-specific inconsistency alignment for domain adaptive object detection. In *Proceedings of the IEEE/CVF Conference on Computer Vision and Pattern Recognition*. 14217–14226.
- [86] Zhen Zhao, Yuhong Guo, Haifeng Shen, and Jieping Ye. 2020. Adaptive object detection with dual multi-label prediction. In *Computer Vision—ECCV 2020: 16th European Conference, Glasgow, UK, August 23–28, 2020, Proceedings, Part XXVIII 16*. Springer, 54–69.
- [87] Zhen Zhao, Yuhong Guo, Haifeng Shen, and Jieping Ye. 2020. Adaptive object detection with dual multi-label prediction. In *Computer Vision—ECCV 2020: 16th European Conference, Glasgow, UK, August 23–28, 2020, Proceedings, Part XXVIII 16*. Springer, 54–69.
- [88] Wenzhang Zhou, Dawei Du, Libo Zhang, Tiejian Luo, and Yanjun Wu. 2022. Multi-granularity alignment domain adaptation for object detection. In *Proceedings of the IEEE/CVF Conference on Computer Vision and Pattern Recognition*. 9581–9590.
- [89] Wenzhang Zhou, Heng Fan, Tiejian Luo, and Libo Zhang. 2023. Unsupervised Domain Adaptive Detection with Network Stability Analysis. In *Proceedings of the IEEE/CVF International Conference on Computer Vision*. 6986–6995.

- [90] Jun-Yan Zhu, Taesung Park, Phillip Isola, and Alexei A Efros. 2017. Unpaired image-to-image translation using cycle-consistent adversarial networks. In *Proceedings of the IEEE international conference on computer vision*. 2223–2232.
- [91] Xinge Zhu, Jiangmiao Pang, Ceyuan Yang, Jianping Shi, and Dahua Lin. 2019. Adapting object detectors via selective cross-domain alignment. In *Proceedings of the IEEE/CVF Conference on Computer Vision and Pattern Recognition*. 687–696.
- [92] Xizhou Zhu, Weijie Su, Lewei Lu, Bin Li, Xiaogang Wang, and Jifeng Dai. 2021. Deformable DETR: Deformable Transformers for End-to-End Object Detection. In *International Conference on Learning Representations*.

A Appendix

A.1 Additional Ablation Studies

In this section, we present additional ablation studies and comparisons to further investigate the effectiveness of our proposed Diffusion Domain Teacher (DDT).

Ablation Study on Unsup Loss Weight λ . We investigate the impact of different unsupervised loss weight λ on cross-domain detection in Tab.11, including Cityscapes [13] to BDD100K [80] ($\text{Cs} \rightarrow \text{B}$), Sim10K [32] to Cityscapes [13] ($\text{S} \rightarrow \text{Cs}$), and VOC [17] to Clipart [30] ($\text{V} \rightarrow \text{Ca}$). Excessively high or low weight λ will degrade the performance of cross-domain detection, so we simply set the parameter λ to 1.

Ablation Study on the Threshold σ of Pseudo Labels. In Tab. 12, we show the impact of different pseudo label threshold σ on the final results. The threshold plays a crucial role in determining the quality of the generated pseudo labels during self-training, and inappropriate threshold will affect cross-domain performance. Ultimately, we choose 0.5 as the default threshold σ setting in all our experiments.

Ablation Study on Data Augmentation of Sup. and Unsup. Branches. We follow previous work [44] and utilize *Strong Augmentation* and *Weak Augmentation* during the self-training process. Tab. 13 presents the impact of *Strong Augmentation* on both supervised and unsupervised data, highlighting the importance of data augmentation in the self-training process.

Ablation Study on Different Versions of Stable Diffusion. In Tab. 14, we present the results of using the popular Stable Diffusion V1.5 (SD-1.5) and the latest version (SD-2.1) respectively. Overall, the results of SD-1.5 are superior to those using SD-2.1, except for the cross-domain detection from Sim10K to BDD100K.

Comparison of Backbone Efficiencies. In Tab. 15, we present a comparative analysis of these models with respect to their architectural sizes, training cost, and inference latency. Diffusion model, with its substantial parameter count and protracted inference time, emerges as an impractical choice for deployment in routine detection tasks within operational settings. Nevertheless, the employment of this model as a strong teacher in self-training framework offers a strategic avenue to leverage its exceptional cross-domain prowess, achieving an average absolute improvement of 21.2 mAP and a relative improvement of 39.7% compared to the baseline, without introducing any additional inference overhead.

Table 11: Ablation Result of Unsup. Loss Weight λ .

λ	$\text{Cs} \rightarrow \text{B}$	$\text{S} \rightarrow \text{Cs}$	$\text{V} \rightarrow \text{Ca}$
0.33	42.7	63.5	54.7
0.50	42.4	63.7	55.3
<u>1.0</u>	43.4	64.0	55.6
2.0	43.0	64.0	53.3
3.0	42.9	63.9	50.0

A.2 Additional Experiments

In this section, we showcase further experiments, including: (1) Cityscapes [13] to FoggyCityscapes [65], aiming to validate the

Table 12: Ablation Result of Threshold σ for Pseudo Labels.

σ	$\text{Cs} \rightarrow \text{B}$	$\text{S} \rightarrow \text{Cs}$	$\text{V} \rightarrow \text{Ca}$
0.3	41.9	63.7	52.4
0.4	42.3	64.2	53.9
<u>0.5</u>	43.4	64.0	55.6
0.6	43.2	62.1	56.1
0.7	43.0	60.3	53.2

Table 13: Ablation Study of Data Augmentation.

Settings of data Aug.	$\text{Cs} \rightarrow \text{B}$	$\text{S} \rightarrow \text{Cs}$	$\text{V} \rightarrow \text{Ca}$
DDT(Ours)	43.4	64.0	55.6
w/o Strong Aug. on Sup.	42.0-1.4	62.0-2.0	54.3-1.3
w/o Strong Aug. on Unsup	42.5-0.9	62.2-1.8	52.3-3.3
w/o All Aug.	42.0-1.4	61.8-2.2	52.1-3.5

Table 14: Ablation Result of Different Stable Diffusion Versions.

Detector	Version	$\text{Cs} \rightarrow \text{B}$	$\text{S} \rightarrow \text{Cs}$	$\text{S} \rightarrow \text{B}$	$\text{V} \rightarrow \text{Ca}$	$\text{V} \rightarrow \text{Co}$	$\text{V} \rightarrow \text{W}$
Diffusion Detector	SD-1.5	32.7	58.2	50.1	47.4	44.4	58.7
	SD-2.1	34.6	58.9	56.4	45.4	42.8	55.2
DDT	<u>SD-1.5</u>	43.4	64.0	58.3	55.6	50.2	63.7
	SD-2.1	42.3	63.4	61.6	53.7	48.9	63.3

results of adverse weather adaptation, and (2) the outcomes of our DDT method employing the FCOS [72] detector, aiming to assess the performance of our approach across different detectors.

Adverse Weather Adaptation from Cityscapes to FoggyCityscapes. We present the result of adverse weather adaptation in Tab. 16. Compared to the baseline, our method with R18, R50, and R101 show improvements of 11.8, 18.0, and 21.6 mAP, respectively. However, our method (50.0 mAP) still falls short of surpassing CMT [3] (50.3 mAP) and HT [15] (50.4 mAP). FoggyCityscapes [65] is a dataset where foggy weather conditions are added to Cityscapes, with similar images and identical labels from Cityscapes. We observe that our DDT method does not demonstrate superior performance in inter-domain as train and test on Cityscapes, which might be the reason for our weaker performance on the FoggyCityscapes compared to the current state-of-the-art results.

Results of Adaptation with FCOS Detector. Previous domain adaptation methods for detection primarily employ the Faster RCNN and FCOS detectors. In main text, we report the results of our method using the Faster RCNN [11] detector. To further validate the effectiveness of our approach, we also present the performance using the FCOS [72] detector in Tab. 17, 18, 19, 20, 21, 22. Overall, the FCOS detector yielded results comparable to the Faster RCNN and outperforms the previous SOTA results in five out of the six datasets, with the exception of Sim10K to Cityscapes where it falls short of HT [15].

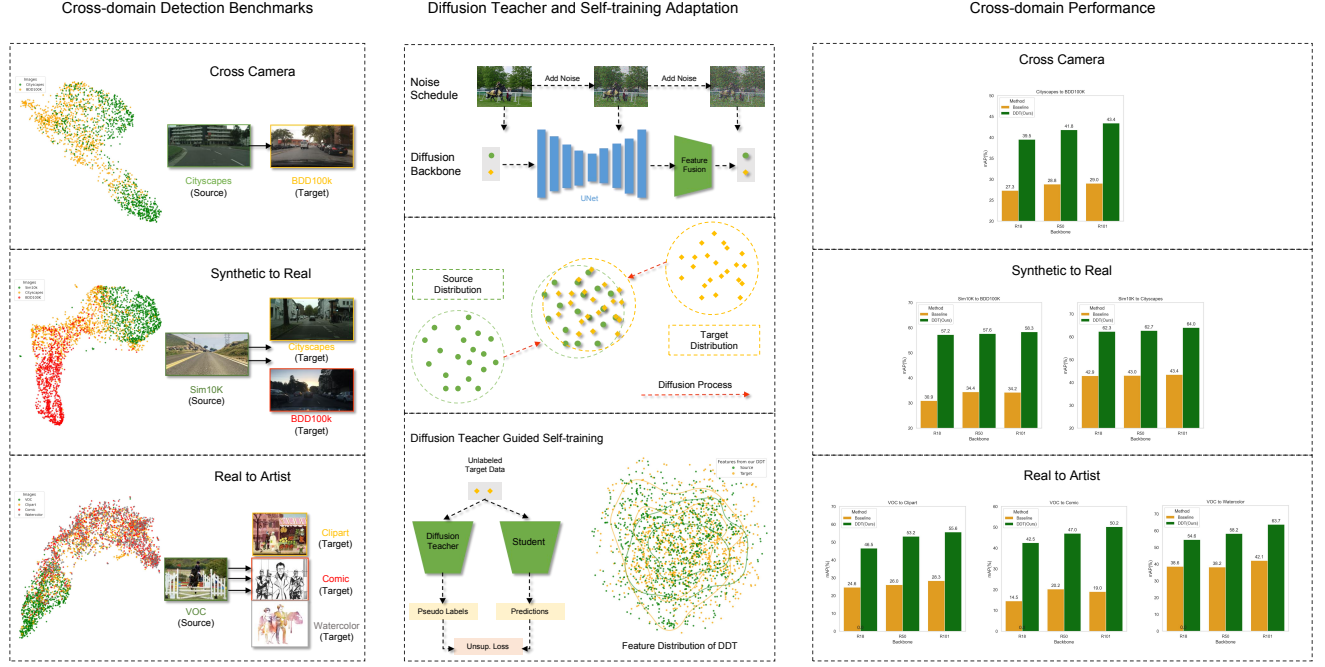


Figure 5: Main content of our work. Left: We present three cross-domain detection benchmarks and visualize the image distributions from source and target domains using the UMAP method. It is evident that there is a large gap between different domains. Middle: We utilize a frozen-weight diffusion model as the backbone to extract features, and employ a detector with the diffusion backbone as the teacher to guide the learning of the student model on the target domain with the self-training framework. Based on the visualization results of the feature distributions, our method significantly reduces the domain gap. Right: Our method substantially enhances the performance of cross-domain object detection without increasing the inference cost.

A.3 Additional visualization results

In Fig. 6, 7, 8, 9, 10, 11, we present additional visualization results for Cityscapes to BDD100K ($Cs \rightarrow B$), Sim10K to BDD100K ($S \rightarrow B$), Sim10K to Cityscapes ($S \rightarrow Cs$), VOC to Clipart ($V \rightarrow Ca$), VOC to Comic ($V \rightarrow Co$), and VOC to Watercolor ($V \rightarrow W$).

Table 15: Results of the efficiency comparison of detectors with different backbones.

Methods	Params (M)	Flops (G)	Train Time (s/iter)	Inference Time (ms/image)	Average Gain (mAP)	Average Rel. Improve (%)
ConvNext-Base [52]	105	401	0.672	73.2	/	/
Swin-Base [51]	104	413	0.693	79.4	/	/
VIT-Base [16]	107	605	0.634	116.5	/	/
MAE (VIT-Base) [16, 22]	107	605	0.634	116.5	/	/
GLIP (Swin-Tiny) [36, 51]	45	198	0.486	84.1	/	/
Diff. (Ours)	991	8,256	1.56	780.4	/	/
DDT (R18)	28	137	0.82	24.6	19.0	38.9
DDT (R50)	41	184	0.90	33.6	21.7	40.1
DDT (R101)	60	262	1.04	40.9	22.9	40.2

Table 16: Quantitative results on adaptation from Cityscapes to FoggyCityscapes. The bold indicates the best results.

Method	Reference	Detector	bus	bicycle	car	mcycle	person	rider	train	truck	mAP
UMT [14]	<i>CVPR'21</i>	FRCNN-R101	56.5	37.3	48.6	30.4	33.0	46.7	46.8	34.1	41.7
IIOB [75]	<i>TPAMI'21</i>	FRCNN-V16	46.1	35.3	49.6	29.9	32.8	44.4	38.0	33.0	38.6
SADA [12]	<i>IJCV'21</i>	FRCNN-R50	50.3	45.4	62.1	32.4	48.5	52.6	31.5	29.5	44.0
CDG [37]	<i>AAAI'21</i>	FRCNN-V16	47.5	38.9	53.1	38.3	38.0	47.4	41.1	34.2	42.3
UaDAN [21]	<i>TMM'21</i>	FRCNN-R50	49.4	38.9	53.6	32.3	36.5	46.1	42.7	28.9	41.1
VDD [76]	<i>ICCV'21</i>	FRCNN-V16	52.0	36.8	51.7	34.2	33.4	44.0	34.7	33.9	40.0
O2Net [19]	<i>ACMMM'22</i>	DETR-R50	47.6	45.9	63.6	38.0	48.7	51.5	47.8	31.1	46.8
SSAL [54]	<i>NeurIPS'22</i>	FCOS	50.0	38.7	59.4	26.0	45.1	47.4	25.7	24.5	39.6
DDF [47]	<i>TMM'22</i>	FRCNN-R50	50.4	39.8	56.1	31.1	37.6	45.5	47.0	30.7	42.3
D-ADAPT [31]	<i>ICLR'22</i>	FRCNN-R50	36.3	46.1	61.7	37.3	44.9	54.2	24.7	25.6	42.2
SCAN [40]	<i>AAAI'22</i>	FCOS-R50	48.6	37.3	57.3	31.0	41.7	43.9	48.7	28.7	42.1
SIGMA [41]	<i>CVPR'22</i>	FCOS-R50	50.4	40.6	60.3	31.7	44.0	43.9	51.5	31.6	44.2
TIA [85]	<i>CVPR'22</i>	FRCNN-V16	52.1	38.1	49.7	37.7	34.8	46.3	48.6	31.1	42.3
TDD [24]	<i>CVPR'22</i>	FRCNN-V16	53.0	49.1	68.2	38.9	50.7	53.7	45.1	35.1	49.2
NLTE [49]	<i>CVPR'22</i>	FRCNN-R50	56.7	43.3	58.7	33.7	43.1	50.7	42.7	33.6	45.4
LODS [38]	<i>CVPR'22</i>	FRCNN-V16	39.7	37.8	48.8	33.2	34.0	45.7	19.6	27.3	35.8
PSN [70]	<i>CVPR'22</i>	FRCNN-V16	48.7	39.2	53.0	33.1	37.4	45.2	38.8	31.1	40.9
MGA [88]	<i>CVPR'22</i>	FCOS-R101	53.2	36.9	61.5	27.9	43.1	47.3	50.3	30.2	43.8
MTTrans [81]	<i>ECCV'22</i>	DETR-R50	45.9	46.5	65.2	32.6	47.7	49.9	33.8	25.8	43.4
OADA [79]	<i>ECCV'22</i>	FCOS-V16	48.5	39.8	62.9	34.3	47.8	46.5	50.9	32.1	45.4
SCAN++ [40]	<i>TMM'22</i>	FCOS-R101	48.1	39.5	57.9	30.1	44.2	43.9	51.2	28.2	42.8
MIC [26]	<i>CVPR'23</i>	FRCNN-R101	52.4	47.5	67.0	40.6	50.9	55.3	33.7	33.9	47.6
SIGMA++ [42]	<i>TPAMI'23</i>	FRCNN-V16	52.2	39.9	61.0	34.8	46.4	45.1	44.6	32.1	44.5
CIGAR [50]	<i>CVPR'23</i>	FCOS-V16	56.6	41.3	62.1	33.7	46.1	47.3	44.3	27.8	44.9
CMT [3]	<i>CVPR'23</i>	FRCNN-V16	66.0	51.2	63.7	41.4	45.9	55.7	38.8	39.6	50.3
HT [15]	<i>CVPR'23</i>	FCOS-V16	55.9	50.3	67.5	40.1	52.1	55.8	49.1	32.7	50.4
Baseline	/	FRCNN-R18	38.6	31.3	45.6	26.1	37.6	45.6	13.9	17.6	32.0
DDT(Ours)	/	FRCNN-R18	49.4	44.0	59.0	36.3	47.9	56.5	27.8	30.0	43.8+ 11.8
Baseline	/	FRCNN-R50	39.1	32.0	42.2	23.8	36.4	44.6	14.7	19.7	31.6
DDT(Ours)	/	FRCNN-R50	53.2	51.5	63.8	44.1	50.3	59.3	41.7	33.1	49.6+ 18.0
Baseline	/	FRCNN-R101	35.7	31.9	41.6	23.8	34.9	41.9	5.7	19.7	29.4
DDT(Ours)	/	FRCNN-R101	53.5	52.2	64.2	43.5	50.9	60.0	42.4	33.6	50.0+ 21.6

Table 17: Quantitative results on adaptation from Cityscapes to BDD100K (Cs→B) with FCOS. The bold indicates the best results.

Method	Reference	Detector	bicycle	bus	car	mcycle	person	rider	truck	mAP
DA-Faster [11]	<i>CVPR'18</i>	FRCNN-V16	22.4	18.0	44.2	14.2	28.9	27.4	19.1	24.9
SWDA [64]	<i>CVPR'19</i>	FRCNN-V16	23.1	20.7	44.8	15.2	29.5	29.9	20.2	26.2
SCDA [91]	<i>CVPR'19</i>	FRCNN-V16	23.2	19.6	44.4	14.8	29.3	29.2	20.3	25.8
CRDA [77]	<i>CVPR'20</i>	FRCNN-R101	25.5	20.6	45.8	14.9	32.8	29.3	22.7	27.4
SED [43]	<i>AAAI'21</i>	FRCNN-V16	25.0	23.4	50.4	18.9	32.4	32.6	20.6	29.0
TDD [24]	<i>CVPR'22</i>	FRCNN-V16	28.8	25.5	53.9	24.5	39.6	38.9	24.1	33.6
PT [10]	<i>ICML'22</i>	FRCNN-V16	28.8	33.8	52.7	23.0	40.5	39.9	25.8	34.9
EPM [27]	<i>ECCV'20</i>	FCOS-R101	20.1	19.1	55.8	14.5	39.6	26.8	18.8	27.8
SIGMA [41]	<i>CVPR'22</i>	FCOS-R50	26.3	23.6	64.1	17.9	46.9	29.6	20.2	32.7
SIGMA++ [42]	<i>TPAMI'23</i>	FRCNN-V16	27.1	26.3	65.6	17.8	47.5	30.4	21.1	33.7
NSA [89]	<i>ICCV'23</i>	FRCNN-V16	/	/	/	/	/	/	/	35.5
HT [15]	<i>CVPR'23</i>	FCOS-V16	38.0	30.6	63.5	28.2	53.4	40.4	27.4	40.2
Baseline	/	FCOS-R18	18.7	12.6	49.0	11.0	40.1	23.4	14.5	24.2
DDT(Ours)			35.7	26.2	63.2	24.3	53.5	35.7	27.0	37.9+ 13.7
Baseline	/	FCOS-R50	21.7	15.9	49.1	13.7	40.4	26.6	14.6	26.0
DDT(Ours)			38.0	32.0	64.0	25.9	55.9	36.8	29.3	40.3+ 14.3
Baseline	/	FCOS-R101	27.0	16.4	51.4	14.7	44.0	28.8	21.2	29.1
DDT(Ours)			37.9	36.1	64.5	30.8	56.9	38.7	31.8	42.4+ 13.3

Table 18: Quantitative results on adaptation from Sim10K to BDD100K (S→B) with FCOS. The bold indicates the best results.

Method	Reference	Detector	mAP(car)
SWDA [64]	<i>CVPR'19</i>	FRCNN-V16	42.9
CDN [68]	<i>ECCV'20</i>	FRCNN-V16	45.3
Baseline	/	FCOS-R18	36.5
DDT(Ours)			56.0+ 19.5
Baseline			38.7
DDT(Ours)	/	FCOS-R50	56.2+ 17.5
Baseline			36.5
DDT(Ours)			57.4+ 20.9

Table 19: Quantitative results on adaptation from Sim10K to Cityscapes (S→Cs) with FCOS. The bold indicates the best results.

Method	Reference	Detector	mAP(car)
DA-Faster [11]	<i>CVPR'18</i>	FRCNN-V16	39.0
SWDA [64]	<i>CVPR'19</i>	FRCNN-V16	40.7
HTCN [7]	<i>CVPR'20</i>	FRCNN-R101	42.5
UMT [14]	<i>CVPR'21</i>	FRCNN-R101	43.1
SSAL [54]	<i>NeurIPS'22</i>	FCOS-R50	51.8
O2NET [19]	<i>ACMMM'22</i>	DDETR-R50	54.1
DDF [47]	<i>TMM'22</i>	FRCNN-R50	44.3
D-ADAPT [31]	<i>ICLR'22</i>	FRCNN-R50	51.9
SCAN [40]	<i>AAAI'22</i>	FCOS-V16	52.6
MTTrans [81]	<i>ECCV'22</i>	DDETR-R50	57.9
SIGMA [41]	<i>CVPR'22</i>	FCOS-R50	53.7
TDD [42]	<i>CVPR'22</i>	FRCNN-V16	53.4
MGA [88]	<i>CVPR'22</i>	FCOS-R101	54.1
OADA [79]	<i>ECCV'22</i>	FCOS-V16	59.2
SIGMA++ [42]	<i>TPAMI'23</i>	FCOS-V16	53.7
CIGAR [50]	<i>CVPR'23</i>	FCOS-V16	58.5
NSA [89]	<i>ICCV'23</i>	FRCNN-V16	56.3
HT [15]	<i>CVPR'23</i>	FRCNN-V16	65.5
Baseline	/	FCOS-R18	47.0
DDT(Ours)			61.4+ 14.4
Baseline			48.4
DDT(Ours)	/	FCOS-R50	62.5+ 14.1
Baseline			51.5
DDT(Ours)			63.5+ 12.0

Table 20: Quantitative results on adaptation from VOC to Comic (V→Co) with FCOS. The bold indicates the best results.

Method	Reference	Detector	bicycle	bird	car	cat	dog	person	mAP
DA-Faster [11]	<i>CVPR'18</i>	FRCNN-V16	31.1	10.3	15.5	12.4	19.3	39.0	21.2
SWDA [64]	<i>CVPR'19</i>	FRCNN-V16	36.4	21.8	29.8	15.1	23.5	49.6	29.4
STABR [33]	<i>CVPR'19</i>	SSD-V16	50.6	13.6	31.0	7.5	16.4	41.4	26.8
MCRA [86]	<i>ECCV'20</i>	FRCNN-V16	47.9	20.5	37.4	20.6	24.5	50.2	33.5
I3Net [8]	<i>CVPR'21</i>	SSD-V16	47.5	19.9	33.2	11.4	19.4	49.1	30.1
DBGL [5]	<i>ICCV'21</i>	FRCNN-R101	35.6	20.3	33.9	16.4	26.6	45.3	29.7
D-ADAPT [31]	<i>ICLR'22</i>	FRCNN-R101	52.4	25.4	42.3	43.7	25.7	53.5	40.5
Baseline	/	FCOS-R18	17.7	7.1	8.3	2.4	5.7	25.3	11.1
DDT(Ours)			54.2	26.6	45.5	29.8	34.4	72.2	43.8+ 32.7
Baseline			20.9	7.2	11.3	4.7	7.9	27.0	13.2
DDT(Ours)	/	FCOS-R50	55.1	32.2	51.4	33.8	38.7	74.6	47.6+ 34.4
Baseline			26.0	9.5	15.4	7.3	8.0	29.3	15.9
DDT(Ours)			55.6	38.2	55.6	36.6	48.1	75.9	51.6+ 35.7

Table 21: Quantitative results on adaptation from VOC to Watercolor (V→W) with FCOS. The bold indicates the best results.

Method	Reference	Detector	bicycle	bird	car	cat	dog	person	mAP
SWDA [11]	<i>CVPR'19</i>	FRCNN-V16	82.3	55.9	46.5	32.7	35.5	66.7	53.3
MCRA [87]	<i>ECCV'20</i>	FRCNN-V16	87.9	52.1	51.8	41.6	33.8	68.8	56.0
UMT [14]	<i>CVPR'21</i>	FRCNN-R101	88.2	55.3	51.7	39.8	43.6	69.9	58.1
IIOD [75]	<i>TPAMI'21</i>	FRCNN-V16	95.8	54.3	48.3	42.4	35.1	65.8	56.9
I3Net [8]	<i>CVPR'21</i>	SSD-V16	81.1	49.3	46.2	35.0	31.9	65.7	51.5
SADA [12]	<i>IJCV'21</i>	FRCNN-R50	82.9	54.6	52.3	40.5	37.7	68.2	56.0
CDG [37]	<i>AAAI'21</i>	FRCNN-V16	97.7	53.1	52.1	47.3	38.7	68.9	59.7
VDD [76]	<i>ICCV'21</i>	FRCNN-V16	90.0	56.6	49.2	39.5	38.8	65.3	56.6
DBGL [5]	<i>ICCV'21</i>	FRCNN-R101	83.1	49.3	50.6	39.8	38.7	61.3	53.8
AT [44]	<i>CVPR'22</i>	FRCNN-V16	93.6	56.1	58.9	37.3	39.6	73.8	59.9
LODS [38]	<i>CVPR'22</i>	FRCNN-R101	95.2	53.1	46.9	37.2	47.6	69.3	58.2
Baseline	/	FCOS-R18	69.8	34.9	37.8	23.3	16.0	48.7	38.4
DDT(Ours)			80.3	60.1	52.5	42.4	34.3	75.8	57.6+ 19.2
Baseline			66.9	42.4	44.6	21.5	13.7	48.3	39.6
DDT(Ours)	/	FCOS-R50	94.4	63.1	51.8	40.8	34.3	75.9	60.1+ 20.5
Baseline			64.0	44.3	41.8	25.7	21.5	53.6	41.8
DDT(Ours)			96.9	65.6	55.4	49.6	40.5	77.2	64.2+ 22.4

Table 22: Quantitative results on adaptation from VOC to Clipart (V→Ca) with FCOS. The bold indicates the best results.

Method	Reference	Detector	aero	bcycle	bird	boat	bottle	bus	car	cat	chair	cow	table	dog	horse	bike	psn	plant	sheep	sofa	train	tv	mAP
SWDA [64]	<i>CVPR'19</i>	FRCNN-V16	26.2	48.5	32.6	33.7	38.5	54.3	37.1	18.6	34.8	58.3	17.0	12.5	33.8	65.5	61.6	52.0	9.3	24.9	54.1	49.1	38.1
CRDA [77]	<i>CVPR'20</i>	FRCNN-R101	28.7	55.3	31.8	26.0	40.1	63.6	36.6	9.4	38.7	49.3	17.6	14.1	33.3	74.3	61.3	46.3	22.3	24.3	49.1	44.3	38.3
HTCN [7]	<i>CVPR'20</i>	FRCNN-R101	33.6	58.9	34.0	23.4	45.6	57.0	39.8	12.0	39.7	51.3	21.1	20.1	39.1	72.8	63.0	43.1	19.3	30.1	50.2	51.8	40.3
SAPNet [35]	<i>ECCV'20</i>	FRCNN-R101	27.4	70.8	32.0	27.9	42.4	63.5	47.5	14.3	48.2	46.1	31.8	17.9	43.8	68.0	68.1	49.0	18.7	20.4	55.8	51.3	42.2
UMT [14]	<i>CVPR'21</i>	FRCNN-R101	39.6	59.1	32.4	35.0	45.1	61.9	48.4	7.5	46.0	67.6	21.4	29.5	48.2	75.9	70.5	56.7	25.9	28.9	39.4	43.6	44.1
IIOD [75]	<i>TPAMI'21</i>	FRCNN-V16	41.5	52.7	34.5	28.1	43.7	58.5	41.8	15.3	40.1	54.4	26.7	28.5	37.7	75.4	63.7	48.7	16.5	30.8	54.5	48.7	42.1
SADA [12]	<i>IJCV'21</i>	FRCNN-R50	29.4	56.8	30.6	34.0	49.5	50.5	47.7	18.7	48.5	64.4	20.3	29.0	42.3	84.1	73.4	37.4	20.5	39.8	41.2	48.0	43.3
UaDAN [21]	<i>TMM'21</i>	FRCNN-R50	35.0	72.7	41.0	24.4	21.3	69.8	53.5	2.3	34.2	61.2	31.0	29.5	47.9	63.6	62.2	61.3	13.9	7.6	48.6	23.9	40.2
DBGL [5]	<i>ICCV'21</i>	FRCNN-R50	28.5	52.3	34.3	32.8	38.6	66.4	38.2	25.3	39.9	47.4	23.9	17.9	38.9	78.3	61.2	51.7	26.2	28.9	56.8	44.5	41.6
AT [44]	<i>CVPR'22</i>	FRCNN-V16	33.8	60.9	38.6	49.4	52.4	53.9	56.7	7.5	52.8	63.5	34.0	25.0	62.2	72.1	77.2	57.7	27.2	52.0	55.7	54.1	49.3
D-ADAPT [31]	<i>ICLR'22</i>	FRCNN-R50	56.4	63.2	42.3	40.9	45.3	77.0	48.7	25.4	44.3	58.4	31.4	24.5	47.1	75.3	69.3	43.5	27.9	34.1	60.7	64.0	49.0
TIA [85]	<i>CVPR'22</i>	FRCNN-R101	42.2	66.0	36.9	37.3	43.7	71.8	49.7	18.2	44.9	58.9	18.2	29.1	40.7	87.8	67.4	49.7	27.4	27.8	57.1	50.6	46.3
LODS [38]	<i>CVPR'22</i>	FRCNN-R101	43.1	61.4	40.1	36.8	48.2	45.8	48.3	20.4	44.8	53.3	32.5	26.1	40.6	86.3	68.5	48.9	25.4	33.2	44.0	56.5	45.2
CIGAR [50]	<i>CVPR'23</i>	FCOS-R101	35.2	55.0	39.2	30.7	60.1	58.1	46.9	31.8	47.0	61.0	21.8	26.7	44.6	52.4	68.5	54.4	31.3	38.8	56.5	63.5	46.2
CMT [3]	<i>CVPR'23</i>	FRCNN-V16	39.8	56.3	38.7	39.7	60.4	35.0	56.0	7.1	60.1	60.4	35.8	28.1	67.8	84.5	80.1	55.5	20.3	32.8	42.3	38.2	47.0
Baseline	/	FCOS-R18	18.7	26.0	15.0	10.1	19.5	65.6	30.6	1.8	24.3	4.2	24.1	7.9	24.9	42.1	33.5	26.1	0.2	17.2	23.0	11.2	21.3
DDT(Ours)			48.9	58.9	32.3	30.0	42.4	72.4	54.5	11.2	48.6	38.9	30.2	27.5	40.1	87.7	76.0	53.2	33.5	38.8	49.5	47.1	46.1+ 24.8
Baseline	/	FCOS-R50	40.0	26.7	17.8	21.0	31.9	32.2	28.8	12.2	36.3	35.7	28.3	6.1	25.5	43.1	37.2	33.5	5.1	25.6	24.5	26.3	26.9
DDT(Ours)			50.7	53.1	34.1	41.5	57.0	86.3	57.1	9.3	49.5	52.8	33.6	32.4	49.0	93.1	82.1	57.8	37.1	42.6	54.1	60.8	51.7+ 24.8
Baseline	/	FCOS-R101	33.6	42.3	21.2	20.1	32.9	62.0	30.0	14.5	41.1	17.9	33.0	9.1	30.4	46.5	39.1	37.4	8.8	22.6	27.3	16.1	29.3
DDT(Ours)			58.6	73.2	42.0	48.0	54.7	84.7	65.2	17.0	55.9	49.4	35.5	40.5	58.6	84.8	82.9	58.0	39.1	41.7	54.7	61.3	55.3+ 26.0

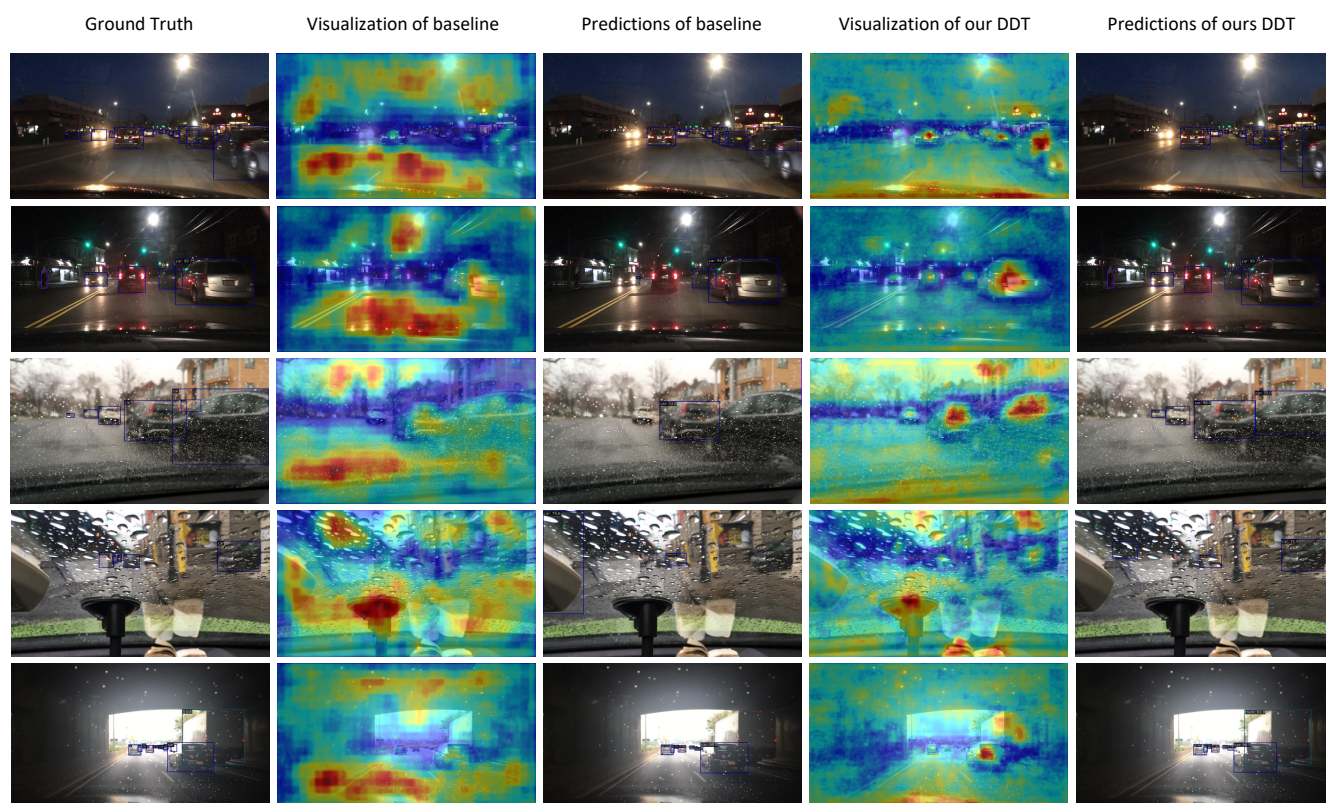


Figure 6: Qualitative prediction results and feature visualization of baseline and our DDT from Cityscapes to BDD100K.

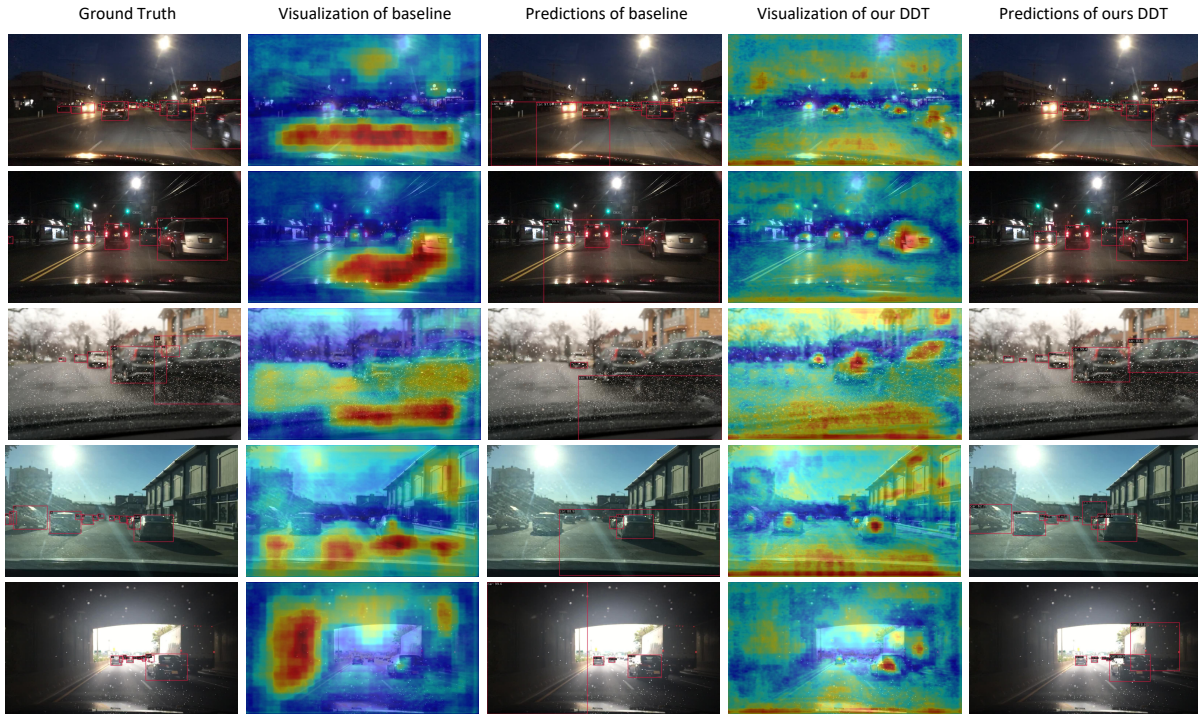


Figure 7: Qualitative prediction results and feature visualization of baseline and our DDT from Sim10K to BDD100K.

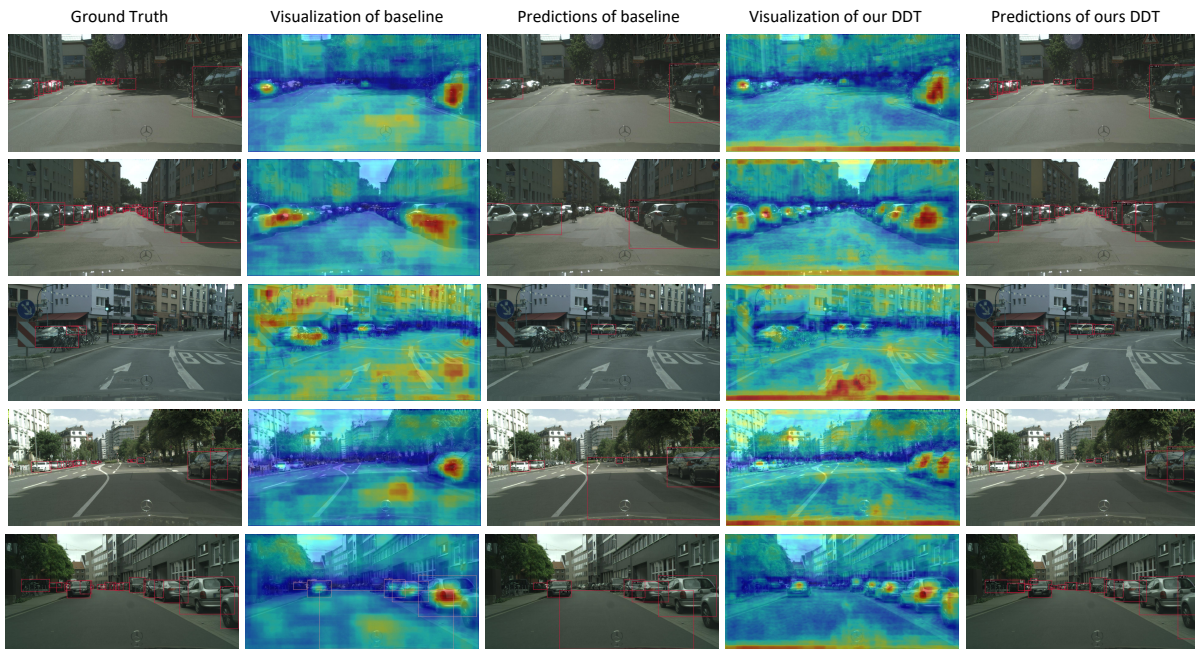


Figure 8: Qualitative prediction results and feature visualization of baseline and our DDT from Sim10K to Cityscapes.

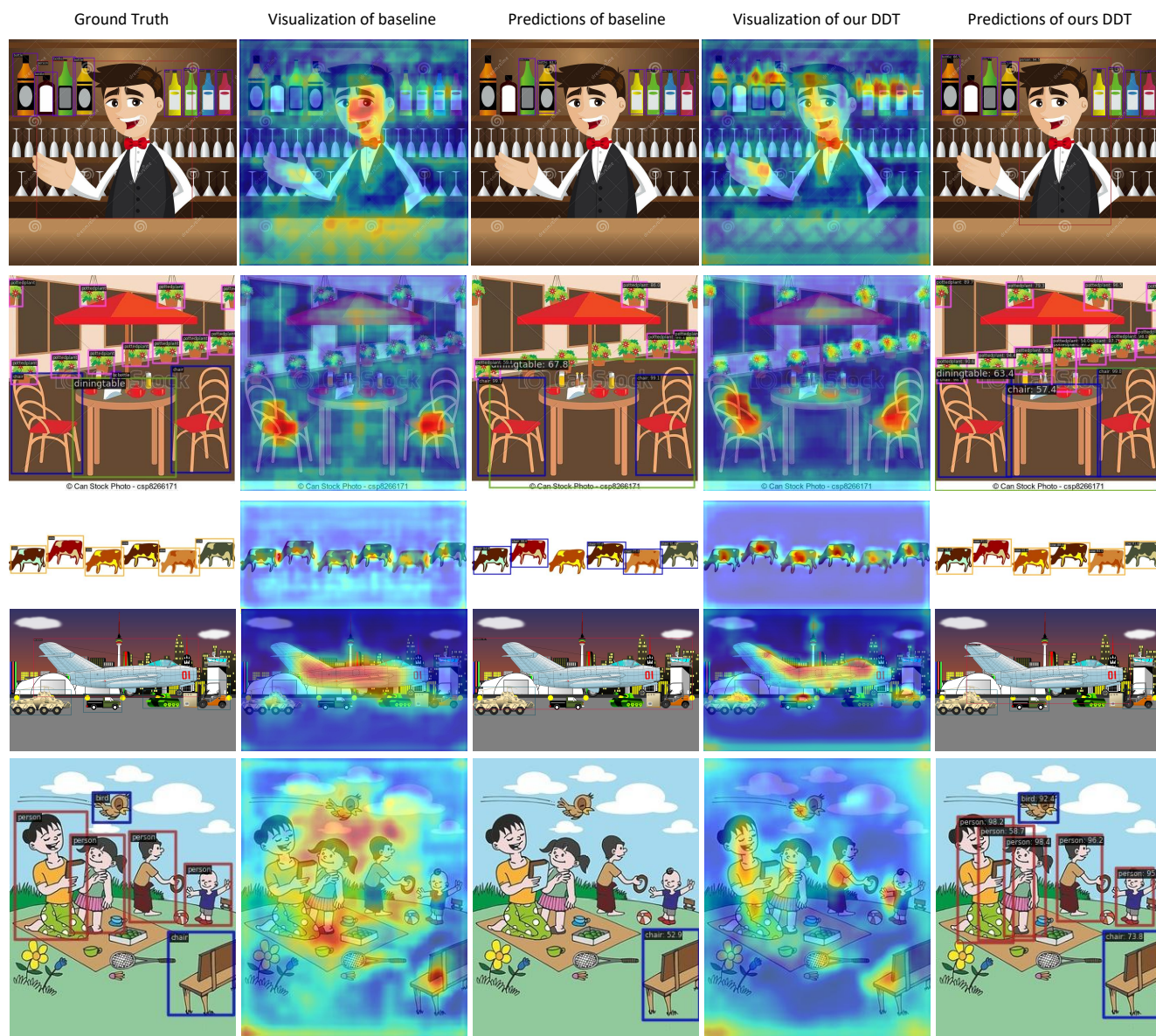


Figure 9: Qualitative prediction results and feature visualization of baseline and our DDT from VOC to Clipart.

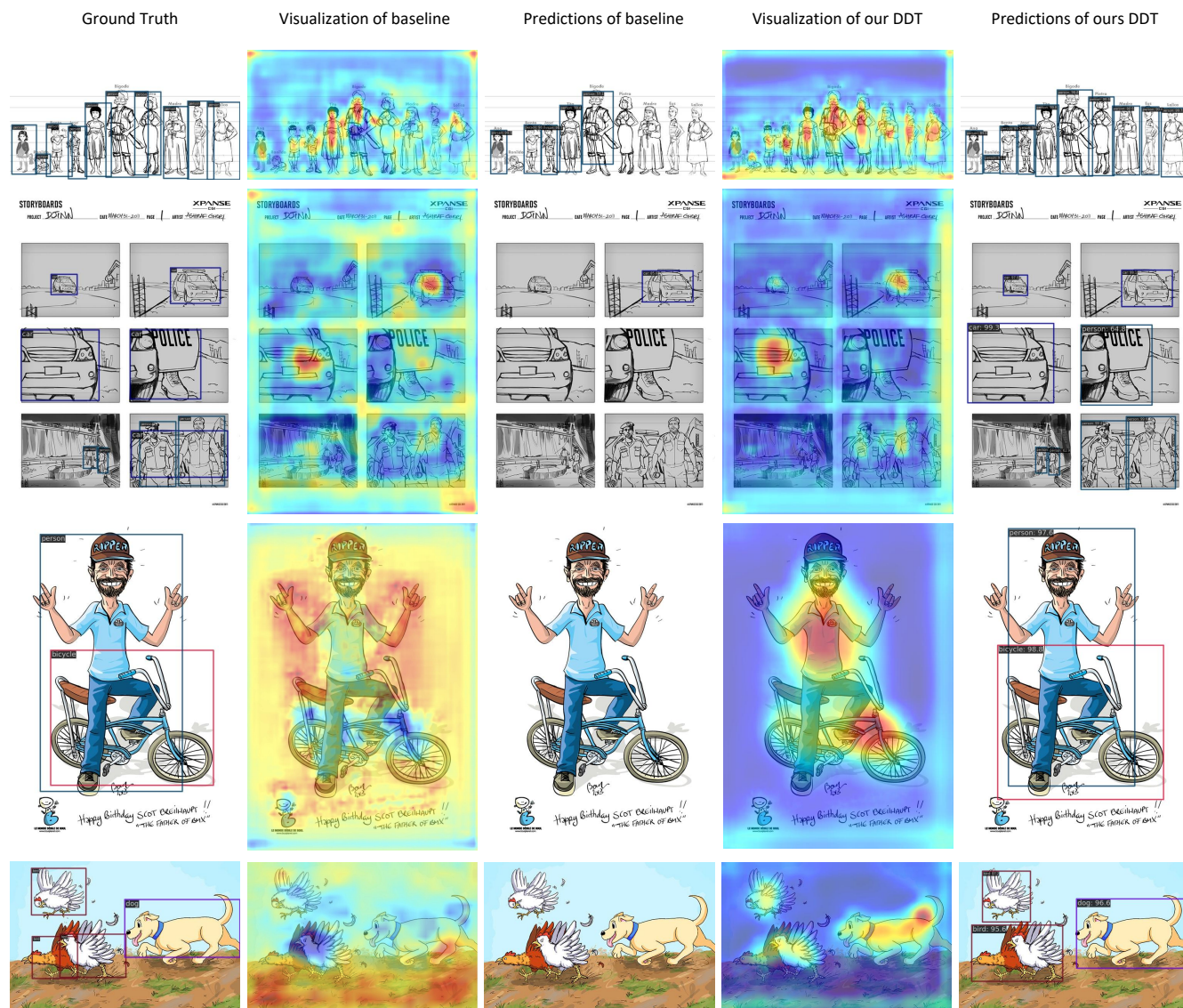


Figure 10: Qualitative prediction results and feature visualization of baseline and our DDT from VOC to Comic.

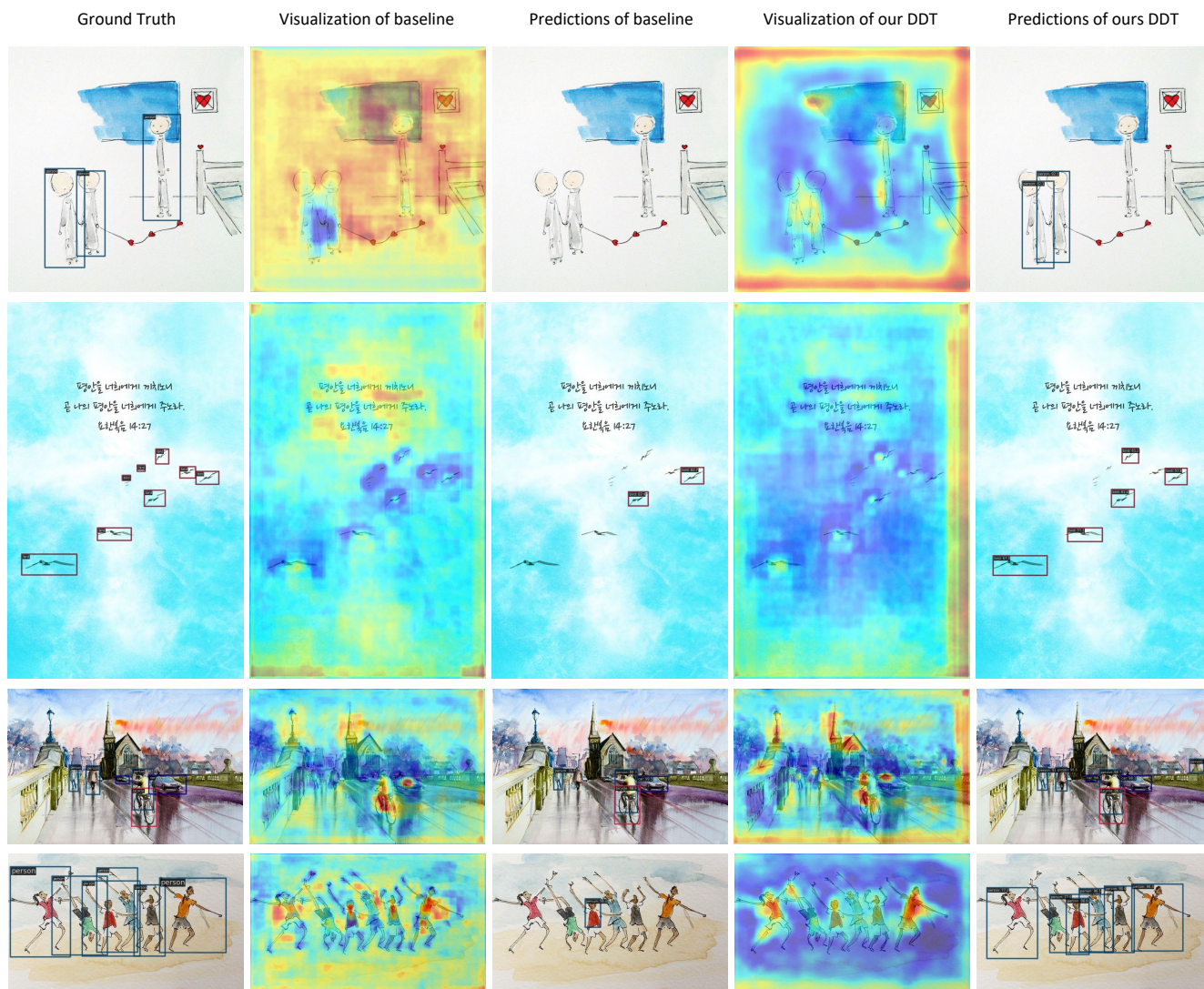


Figure 11: Qualitative prediction results and feature visualization of baseline and our DDT from VOC to Watercolor.